JVI Journals.ASM.org

The Kissing-Loop T-Shaped Structure Translational Enhancer of *Pea Enation Mosaic Virus* Can Bind Simultaneously to Ribosomes and a 5′ Proximal Hairpin

Feng Gao,[a] Suna P. Gulay,[a] Wojciech Kasprzak,[b] Jonathan D. Dinman,[a] Bruce A. Shapiro,[c] Anne E. Simon[a]

Department of Cell Biology and Molecular Genetics, University of Maryland College Park, College Park, Maryland, USA[a]; Basic Science Program, SAIC-Frederick, Inc., Center for Cancer Research Nanobiology Program, Frederick National Laboratory for Cancer Research, Frederick, Maryland, USA[b]; Center for Cancer Research Nanobiology Program, National Cancer Institute, Frederick, Maryland, USA[c]

The *Pea enation mosaic virus* (PEMV) 3′ translational enhancer, known as the kissing-loop T-shaped structure (kl-TSS), binds to 40S subunits, 60S subunits, and 80S ribosomes, whereas the *Turnip crinkle virus* (TCV) TSS binds only to 60S subunits and 80S ribosomes. Using electrophoretic mobility gel shift assay (EMSA)-based competition assays, the kl-TSS was found to occupy a different site in the ribosome than the P-site-binding TCV TSS, suggesting that these two TSS employ different mechanisms for enhancing translation. The kl-TSS also engages in a stable, long-distance RNA-RNA kissing-loop interaction with a 12-bp 5′-coding-region hairpin that does not alter the structure of the kl-TSS as revealed by molecular dynamics simulations. Addition of the kl-TSS in *trans* to a luciferase reporter construct containing either wild-type or mutant 5′ and 3′ PEMV sequences suppressed translation, suggesting that the kl-TSS is required in *cis* to function, and both ribosome-binding and RNA interaction activities of the kl-TSS contributed to translational inhibition. Addition of the kl-TSS was more detrimental for translation than an adjacent eIF4E-binding 3′ translational enhancer known as the PTE, suggesting that the PTE may support the ribosome-binding function of the kl-TSS. Results of in-line RNA structure probing, ribosome filter binding, and high-throughput selective 2′-hydroxyl acylation analyzed by primer extension (hSHAPE) of rRNAs within bound ribosomes suggest that kl-TSS binding to ribosomes and binding to the 5′ hairpin are compatible activities. These results suggest a model whereby posttermination ribosomes/ribosomal subunits bind to the kl-TSS and are delivered to the 5′ end of the genome via the associated RNA-RNA interaction, which enhances the rate of translation reinitiation.

Cellular gene expression is regulated at multiple steps, including when mRNAs are translated into proteins. Posttranscriptional control of gene expression includes events that occur during translation initiation, when the correct start codon is identified and decoded (1, 2). Canonical translation initiation in eukaryotes is a complex, multistep process in which the 5′ m7GpppN cap and 3′ poly(A) tail cooperate to recruit translation initiation factors and ribosomal subunits. The 5′ cap is recognized by the cap-binding protein eIF4E, which along with the scaffold protein eIF4G is one subunit of the eukaryotic translation initiation factor complex eIF4F (3). Simultaneous binding of eIF4G to eIF4E and poly(A)-binding protein forms a bridge that circularizes the mRNA, which is thought to recycle ribosomes, leading to more efficient translation (4). The 43S ribosome preinitiation complex (PIC), consisting of the 40S ribosomal subunit- and Met-tRNA-containing ternary complex, is recruited to the 5′ end of mRNA via the interaction between eIF4G and additional initiation factors (3, 5). The PIC then scans the message in a 5′-to-3′ direction until contacting an initiation codon in the proper context. The 60S ribosomal subunit joins to form the 80S ribosome-mRNA complex, and translation elongation commences with the entry of the appropriate aminoacylated tRNA complex into the ribosome A site.

Nonconventional mechanisms of translation operate during cellular stress and are also utilized by mRNAs lacking a 5′ cap and/or a 3′ poly(A) tail (1, 6). Cap-independent ribosome entry is frequently studied using animal RNA viruses that have replaced the 5′ cap with highly structured, *cis*-acting elements known as internal ribosome entry sites (IRESs) that encompass or are near the initiation codon (7). Attraction of the small ribosomal subunit to different viral IRESs usually requires a subset of initiation factors but can also occur in the absence of factors (8, 9). In contrast with animal RNA viruses, plant RNA viruses whose genomes lack a 5′ cap and 3′ poly(A) tail have short 5′-untranslated regions (5′UTRs) that do not contain similar highly structured IRES elements. Translation of plant RNA viruses in the family *Tombusviridae* requires distinctive cap-independent translation enhancers (CITEs) located within the viral genomic RNA's 3′UTR and nearby coding region (10). 3′CITEs are currently divided into at least eight classes, based mainly on their secondary structures, including Y-shaped, I-shaped, BTE-like, and TED-like structures (11). 3′CITEs are bound by various translation initiation factors and are generally associated with a long-distance, kissing-loop interaction that connects the 3′CITE with the 5′UTR, resulting in genome circularization that delivers the bound factors to the viral 5′ end (12–15). How and when the 3′CITE-bound factors contribute to ribosome recruitment and how ribosomes are delivered to or near the 5′ terminus before scanning to the initiation codon (16–18) are not known.

tRNA-like structures that exist either internally or at the 3′

Received 18 July 2013 Accepted 23 August 2013
Published ahead of print 28 August 2013
Address correspondence to Bruce A. Shapiro, shapirbr@mail.nih.gov, or Anne E. Simon, simona@umd.edu.

doi:10.1128/JVI.02005-13

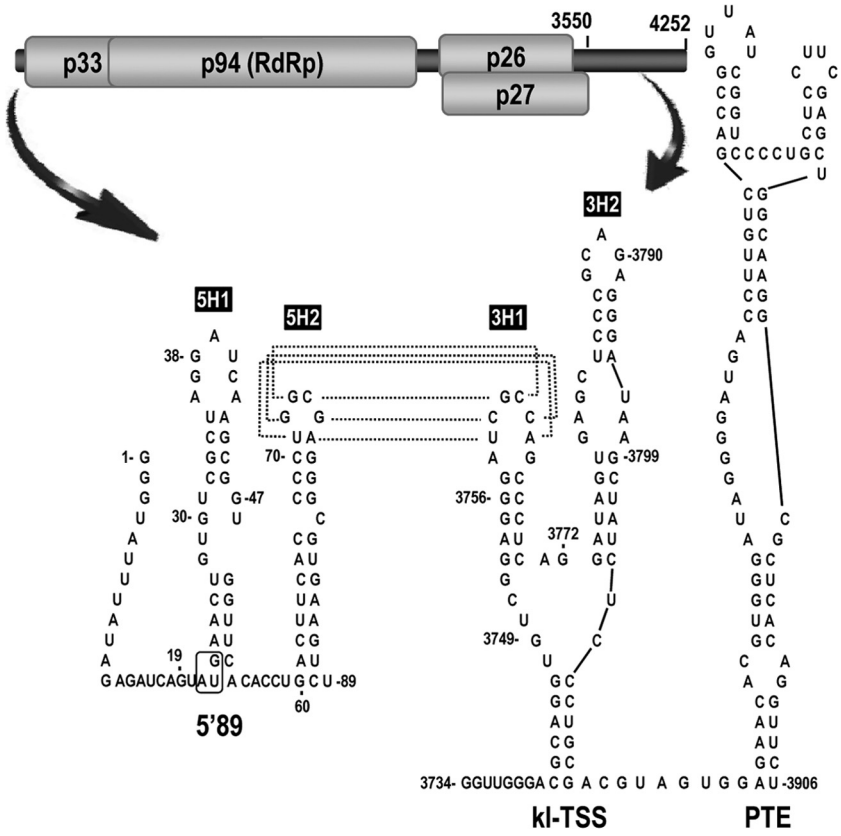

FIG 1 The two adjacent 3′CITEs in the 3′UTR of PEMV. (Top) Genome organization of PEMV. (Bottom) Secondary structures of the 5′-terminal 89 nt (5′89) and the kl-TSS and PTE 3′CITEs. The long-distance kissing-loop interaction between 5′89 hairpin 5H2 and kl-TSS hairpin 3H1 (dashed lines) has been confirmed experimentally (12). The p33 initiation codon at the base of hairpin 5H1 is boxed.

termini of RNA virus genomes have a variety of functions, including being used as 3′CITEs. Some capped, positive-strand RNA plant viruses, including tymo-, bromo-, and tobamoviruses, contain 3′-terminal tRNA-like structures that are aminoacylated by host aminoacyl tRNA-synthetases and function in replication, translation, packaging, and fidelity of the genome (19). The retrovirus HIV-1 contains an internal tRNA anticodon stem-like element that mimics the anticodon loop of $tRNA^{Lys}$ and functions to increase the efficiency with which $tRNA^{Lys3}$ anneals to the viral genome during replication (20). Other examples of tRNA mimicry in RNA viruses include a replication enhancer in the RNA3 intergenic region of *Brome mosaic virus* and related cucomoviruses, which is a substrate for tRNA modification enzymes *in vivo* (21), and the IRES of *Cricket paralysis virus*, which interacts with the ribosome's decoding groove by mimicking the tRNA anticodon-mRNA codon interaction (22).

An internally located tRNA mimic that forms from three hairpins and two pseudoknots functions as a 3′CITE in the carmovirus *Turnip crinkle virus* (TCV) (family *Tombusviridae*) (23, 24). The TCV T-shaped structure (TSS) binds to 80S ribosomes and 60S ribosomal subunits in the vicinity of the P site (23) and is not associated with any long-distance kissing-loop interaction. Rather, circularization of the genome may result from 60S subunits bound to the 3′UTR TSS joining 40S subunits bound to a pyrimidine-rich sequence in the 5′UTR (25). A second tRNA mimic that functions as a 3′CITE was recently discovered in the 3′UTR of *Pea enation mosaic virus* (PEMV). PEMV is a bipartite virus with two single-stranded plus-sense RNAs that were originally independent viruses (26). PEMV RNA 2 (called PEMV throughout this report) is classified as an umbravirus and is missing the 5′ cap and poly(A) tail, similar to viruses in the *Tombusviridae* family. PEMV is a recombinant virus of 4.2 kb that encodes a carmovirus-like RNA-dependent RNA polymerase (RdRp) and two overlapping, movement-associated proteins (p26 and p27) originating from a second, unknown virus (27). PEMV replicates independently in pea protoplasts but requires products encoded by the associated viral RNA for encapsidation and transmission from plant to plant (27).

The central region of the PEMV 3′UTR (703 nucleotides [nt]) contains a 3′CITE known as a *Panicum mosaic virus* (PMV)-like enhancer, or PTE (12, 28) (Fig. 1). The PEMV PTE binds to eIF4E, and its binding efficiency correlates with translational enhancement (29, 30). Although PTEs found in the 3′UTRs of seven carmoviruses are known or postulated to engage in long-distance kissing-loop interactions with hairpins in the 5′UTR or nearby coding sequences (13), the PEMV PTE relies on an adjacent, upstream element for relocalization of itself and bound initiation factors to the 5′ end (12). The upstream element contains a two-hairpin, three-way branched secondary structure with the 5′-side hairpin (3H1) participating in a kissing-loop interaction with a 12-bp hairpin (5H2) located near the 5′ end of the p33 open reading frame (ORF) (Fig. 1). This 3′UTR branched element was pre-

dicted to fold into a TSS and was therefore designated a "kissing-loop TSS" (kl-TSS) (12). Similar to the TCV TSS, the PEMV kl-TSS binds to 80S ribosomes and 60S ribosomal subunits; however, unlike the TCV TSS, the kl-TSS also binds to 40S subunits (12). Since both ribosome-binding and long-distance RNA-RNA interaction activities of the kl-TSS are important for efficient translation, the kl-TSS has been designated a 3′CITE.

In this study, we determined that the kl-TSS inhibits translation more efficiently than the associated PTE when added to a reporter template in *trans* and that both RNA-RNA interaction and ribosome-binding activities contribute to translational inhibition. In addition, we found that the kl-TSS and TCV TSS occupy different sites in the 80S ribosome and that the kl-TSS can simultaneously bind to ribosomes and interact with the 5′ hairpin, leading to a reevaluation of the orientation of the kl-TSS with respect to canonical tRNAs. These results suggest that (i) the PTE may contribute to kl-TSS ribosome binding and is not associated with an independent function, (ii) RNA viruses have evolved at least two different mechanisms for using TSS-type 3′CITEs, and (iii) the RNA-RNA interaction of the kl-TSS can directly place bound ribosomes/ribosomal subunits at the 5′ end for reinitiation of translation.

MATERIALS AND METHODS

***In vitro* translation and *trans*-inhibition assays.** The translation reporter construct (firefly luciferase [Fluc] flanked by the PEMV 5′ 89 nt [5′89] and 3′UTR [703 nt]) was described previously (12). *In vitro* translation using wheat germ extracts (WGE) (Promega) was performed using 3 pmol of *in vitro*-synthesized transcripts in a 15-μl translation assay mixture according to the manufacturer's instructions. After incubation at 25°C for 1 h, luciferase activity was measured using a luciferase assay reporter system (Promega) and a Modulus microplate multimode reader (Turner BioSystems). For *trans*-inhibition assays, 30 pmol of competitor RNA was added to the reaction mixture. Competitor transcripts were synthesized from PCR fragments, using wild-type (wt) or mutated PEMV (pUC19-PEMV) as a template with 5′ primers that contained a T7 RNA polymerase promoter.

EMSAs. Electrophoretic mobility gel shift assays (EMSAs) were performed as described previously (12). Typical reaction mixtures contained 3 pmol of *in vitro*-transcribed PEMV kl-TSS or TCV TSS that was labeled at the 5′ end with [γ-^{32}P]ATP and polynucleotide kinase, 12 pmol of *Arabidopsis* 80S ribosomes, and a 1- to 10-fold molar excess of unlabeled competing RNA in ribosome binding buffer [80 mM HEPES, pH 7.5, 160 mM NH_4Cl, 11 mM $Mg(CH_3COO)_2$, 6 mM β-mercaptoethanol, 0.4 mM GTP, 2 mM spermidine, 0.4 μg/ml of poly(U)]. After incubation at 25°C for 30 min, the reaction mixture was resolved by electrophoresis in native composite gels [0.5% agarose and 3% acrylamide in 1× TBM buffer, composed of 89 mM Tris, 89 mM boric acid, and 10 mM $Mg(CH_3COO)_2$] at 4°C. After electrophoresis, gels were dried and exposed to X-ray film.

Purification of 80S ribosomes and 40S/60S ribosomal subunits from *Arabidopsis thaliana* protoplasts. Plant ribosomes and ribosomal subunits were isolated as recently described (32). Briefly, *Arabidopsis* protoplasts prepared from callus cultures were lysed in buffer A (250 mM sucrose, 200 mM Tris-HCl, pH 8.8, 30 mM $MgCl_2$, 50 mM KCl, 1 mM dithiothreitol [DTT], 1 mg/ml heparin) by gently shaking for 15 min on ice. The lysate was subjected to centrifugation at 10,000 × *g* for 1 min. The resulting supernatant was loaded into a 25% glycerol cushion for centrifugation at 4°C for 3 h at 50,000 rpm, using an MLS-50 rotor (Beckman). Ribosome pellets were washed and resuspended in storage buffer [50 mM HEPES-KOH, pH 7.6, 5 mM $Mg(CH_3COO)_2$, 50 mM NH_4Cl, 25% glycerol, 1 mM DTT]. Ribosomes were salt washed to remove any associated tRNAs and translation factors as described previously for yeast ribosomes (23). For purification of plant 40S and 60S ribosomal subunits, purified 80S ribosomes were subjected to sucrose gradient centrifugation, and 40S- or 60S-containing fractions were applied to an Amicon Ultra 100K column (Millipore) to exchange the buffer for storage buffer (23). Ribosomes (2 to 10 pmol/μl) were stored at −80°C.

Ribosome purification from *Saccharomyces cerevisiae*. *Saccharomyces cerevisiae* strain JD1370 (*MAT***a** *trp1 ura3 leu2 PEP4*::*HIS3 NUC1*::*LEU2*) was used for purification of yeast ribosomes for high-throughput selective 2′-hydroxyl acylation analyzed by primer extension (hSHAPE). Ribosome purification was performed as previously described (33), followed by puromycin treatment to remove tRNAs (34). In brief, yeast cells were grown to an optical density at 595 nm (OD_{595}) of 1.0 in 500 ml of yeast extract-peptone-adenine-dextrose (YPAD). Cells were broken using 0.5-mm zirconia-silica beads at 4°C, using a Biospec Mini bead beater. Cellular debris was removed by centrifugation at 30,000 × *g* for 30 min in a Beckman-Coulter Optima Max E ultracentrifuge. Ribosomes in the supernatant were purified using Sulfolink resin (Pierce). After elution from the column, ribosomes were treated with 1 mM GTP and 1 mM puromycin (pH 7.0) at 30°C for 30 min. After overnight centrifugation in a 25% glycerol cushion with a high salt concentration at 100,000 × *g*, the ribosome pellets were collected, quantified spectrophotometrically, and stored at −80°C.

In-line RNA structure probing. In-line probing was performed as previously described (35). Briefly, kl-TSS and 5′89 transcripts were 5′-end labeled with [γ-^{32}P]ATP and polynucleotide kinase and purified by electrophoresis through 5% denaturing polyacrylamide gels. After heating the RNA to 75°C and slow cooling to room temperature, 5 pmol of RNA, either alone or in the presence of a 10-fold molar excess of unlabeled partner RNA and/or 10 pmol of *Arabidopsis* 80S ribosomes or 40S/60S ribosomal subunits, was allowed to self-cleave in 50 mM Tris-HCl (pH 8.5), 20 mM $MgCl_2$ at 25°C for 14 h. At least three independent in-line probing assays were performed, and only reproducible differences are described.

hSHAPE analysis of rRNAs within 80S ribosomes. hSHAPE experiments were conducted using either the kl-TSS alone (250 pmol) or a mixture of kl-TSS (250 pmol) and 5′89 (750 pmol) preincubated together at 30°C for 25 min in SHAPE ribosome buffer (80 mM HEPES, pH 7.5, 50 mM NaCl, 5 mM MgOAc, 6 mM β-mercaptoethanol). Yeast 80S ribosomes (50 pmol) were added to the RNAs and incubated together at 30°C for 30 min. Ribosome-RNA mixtures were divided into two aliquots, and 75 μl of SHAPE ribosome buffer was added to each tube, along with either 12.5 μl of dimethyl sulfoxide (DMSO) or 12.5 μl of 60 mM 1-methyl-7-nitroisatoic anhydride (1M7) (supplied by Kevin Weeks, University of North Carolina). After 10 min of incubation at 30°C, the ribosome-RNA mixture was precipitated overnight in 70% ethanol and 300 mM sodium acetate. Following centrifugation, rRNAs were purified using an RNAqueous Micro kit (Ambion), and concentrations were determined using a Nanodrop 1000 spectrophotometer.

Primer extension reactions were performed as previously described (33). Coverage of the entire 18S and 25S rRNAs was achieved using 20 fluorescently labeled primers (Applied Biosystems) (33). Each primer was labeled with a fluorescent compound (6-carboxyfluorescein [FAM], VIC, NED, or PET) (Applied Biosystems) and diluted to 2.5 pmol/μl. FAM-labeled primers were used for the 1M7-treated samples, VIC-labeled primers were used for the DMSO-treated samples, and NED- and PET-labeled primers were used for sequencing reactions. To 1 μg of rRNA, 2.5 pmol of primer was added, and the samples were brought to 6.5 μl or 5.5 μl (for sequencing samples). The samples were incubated at 65°C for 5 min and then at 50°C for 5 min. A master mix containing 100 U of Superscript 3 reverse transcriptase (Invitrogen), a 10 mM concentration of each deoxynucleoside triphosphate (dNTP), 5× Superscript buffer (Invitrogen), and 100 mM DTT was prepared in a final volume of 10 μl. In addition, a 10 mM concentration of the appropriate dideoxynucleoside triphosphate (ddNTP) was added to the sequencing samples. Samples were incubated at 50°C for 1 min, 52°C for 45 min, and 65°C for 5 min and then placed on ice. The four extension reaction mixtures were combined and precipitated overnight in 100% ethanol at −20°C. Samples were washed twice with 70% ethanol and resuspended in 10 μl Hi-Di formamide (Applied Biosystems). Capillary gel electrophoresis was performed by Genewiz.

ShapeFinder analysis. hSHAPE data were analyzed using ShapeFinder as previously described (33). Data were normalized using Microsoft Excel and assigned to the following levels of reactivity: 0, values lower than a trace's median value; 1, values between the median and the mean; 2, values between the mean and the 1st standard deviation; 3, values between the 1st and 2nd standard deviations; and 4, values above the 2nd standard deviation. The mean, median, and standard deviation were calculated on a per-primer basis. The reactivity data for kl-TSS and kl-TSS-plus-5′89 samples were compared to each other and to hSHAPE results for salt-washed 80S ribosomes alone (33). The differences were plotted in a Postscript file of the two-dimensional (2-D) maps of rRNAs.

Filter binding assays. Filter binding assays were performed as described previously (23). Briefly, 2 to 60 pmol of kl-TSS RNA labeled at the 5′ end with [γ-^{32}P]ATP and polynucleotide kinase was incubated either alone or with a 3-fold molar excess of 5′89 or 5′89$_{5H2m2}$ in ribosome binding buffer [80 mM HEPES, pH 7.5, 160 mM NH_4Cl, 11 mM $Mg(CH_3COO)_2$, 6 mM β-mercaptoethanol, 0.4 mM GTP, 2 mM spermidine, 0.4 μg/ml of poly(U)] at 25°C for 30 min. Following annealing of the RNAs, 15 pmol of *Arabidopsis* 80S ribosomes was added to a total volume of 30 μl, and incubation was continued for an additional 30 min. Ribosome-RNA mixtures were then applied to nitrocellulose membrane filters (Millipore) and washed three times with ribosome binding buffer, and radioactivity was measured by scintillation counting. Data were fitted using GraphPad Prism software, and the K_d (dissociation constant) was calculated from the best-fit curves generated by nonlinear regression. All experiments were conducted in triplicate.

Molecular modeling. Three-dimensional (3-D) structure modeling was performed using the program RNA2D3D (36). This program allows for connecting nucleic acid chains via the program-shaped hairpin loop tertiary interactions. This option was used to model the kissing loop between the RNA2D3D-generated model of 5′89 hairpin 5H2 and hairpin 3H1 of the kl-TSS models, based on the 6-nt complementary sequences in the hairpin loops of the two structures (Fig. 1). The model, kl-TSS/5H2, based on structure A from Fig. 7B in reference 12, is described in detail below, while the details of the alternative structure B-derived model (12) are omitted. Both models were built based on the secondary structure probing data (12). Docking of the kl-TSS hairpin 3H1 with the 5′89 hairpin 5H2 required opening of the U71-A76 base pair in 5H2 and reshaping of the complementary 6-nt segment of the 3H1 loop from the original structure A model (12) by use of the RNA2D3D tool. The initial rough model was energy minimized in Amber (see below). In the process, the G75-C3760 base pair was distorted, whereas the A76-U3759 base pair partly opened up, effectively truncating the kissing-loop interaction to 5 bp. The kl-TSS/5H2 kissing-loop model and the reshaped kl-TSS model were subjected to molecular dynamics (MD) runs to explore the stability of the kissing-loop interaction and to compare the dynamics of the kissing loop-connected model to its kl-TSS-only counterpart.

MD simulations. MD simulations were performed with Amber 12, using the ff10 Cornell force field for RNA and the particle mesh Ewald summation method to calculate the electrostatic interactions (37–40). After the model was subjected to energy minimization, the minimized molecule was solvated in water with Na^+ ions to neutralize the backbone phosphate charges. The kissing complex of kl-TSS and 5H2 consisted of one 71-nt chain (kl-TSS) neutralized with 70 Na^+ ions and one 29-nt chain (5H2), neutralized with an additional 28 Na^+ ions. Neutralized RNA molecules were placed in solvent boxes with TIP3P water molecules, and additional Na^+-Cl^- ion pairs were added to the box to solvate the system to a relative salt concentration of 0.1 M. The equilibration protocol involved solvent equilibration in multiple stages (minimization, heating, and short dynamic stages), with the RNA being subjected to slowly released motion restraints (holding). The entire system was equilibrated at 300 K by using a Berendsen thermostat (41). The last phase of the equilibration, without any restraints on the RNA, was performed for 0.5 ns. A cutoff of 9 Å was used with the nonbonded interactions. SHAKE was applied to all hydrogen bonds in the system. Pressure was maintained at 1.0 Pa by using the Berendsen algorithm (41), and a periodic boundary condition was imposed. Following equilibration, the production simulation was performed with 2-fs time steps to obtain two trajectories, one of 58 ns for the kl-TSS/5H2 model and one of 97 ns for the kl-TSS alone (repeated, because the previous kl-TSS MD simulations were performed with ff99bsc0 [12]). The total size of the kl-TSS/5H2 system was 121,429 atoms (3,221 atoms from the RNA molecules). The total size of the kl-TSS system was 56,799 atoms, with 2,288 atoms from the kl-TSS RNA molecule (see Fig. 8 and 9 for illustrations). The solvent boxes had clearance distances of 15 Å and 10 Å, respectively (clearance distance is the minimum distance between the solute and the solvent box wall, termed "buffer" in Amber). Analyses of the MD results, which included monitoring of the stability of the kissing-loop complex, were performed using the ptraj module of Amber (38). They excluded the equilibration stage output.

RESULTS

Both ribosome-binding and RNA-RNA interaction activities of the kl-TSS contribute to inhibition of translation in *trans*. Assays to identify elements that are necessary for efficient translation frequently make use of reporter constructs and *in vitro* translation systems such as wheat germ extracts (WGE). Some 3′CITEs, however, including the TCV TSS and some tombusvirus YSS elements, do not enhance translation in WGE and other cell-free systems, possibly due to an overabundance of translation factors that are limiting in living cells (23, 42). To determine if the kl-TSS enhances translation in WGE, luciferase reporter transcripts were tested for translation in the presence and absence of mutations disrupting the RNA-RNA interaction (Fig. 2). RNA transcribed from a construct containing the 5′ 89 nt and the 3′UTR (5′89+3U) was translated 10-fold more efficiently than RNA that was missing the 3′UTR (5′89+0) and 6-fold more efficiently than RNA from a construct that contained the 20-nt 5′UTR and the 3′UTR (5′20+3U) (Fig. 2B). Single or two-base alterations in either the 5′ or 3′ kissing-loop sequence in 5′89+3U reduced translation by 2.6- to 6-fold, whereas the combinations of compensatory mutations restored translation to greater than wt levels. These results indicate that the kl-TSS is functional in WGE and that the RNA-RNA kissing-loop interaction between hairpin 5H2 and the kl-TSS is important for efficient translation *in vitro* and in protoplasts, as previously found (12). When the entire 3′UTR (10-fold molar excess) was added in *trans* to WGE containing 5′89+3U, luciferase activity was reduced by 76% compared with levels obtained in the absence of any added transcripts (Fig. 2C). Addition of a fragment containing only the kl-TSS and the adjacent PTE 3′CITE (kl-TSS+PTE) reduced translation of 5′89+3U by a similar level (75%), suggesting that the kl-TSS and PTE are the major WGE-functional 3′CITEs in the 3′UTR of PEMV. The PTE alone produced only a minor (14%) reduction in translation, whereas the kl-TSS alone reduced translation by 57%.

To determine if formation of the kissing-loop interaction between kl-TSS transcripts and 5′89+3U in *trans* interferes with the kl-TSS RNA-RNA interaction in *cis*, 2-nt mutations were introduced into the kl-TSS (kl-TSS$_{3H1m2}$) or kl-TSS+PTE (kl-TSS$_{3H1m2}$+PTE) fragment (Fig. 2A). Loss of the ability to form the RNA-RNA interaction in *trans* reduced but did not eliminate the inhibitory effect of kl-TSS$_{3H1m2}$ or kl-TSS$_{3H1m2}$+PTE, with translation still reduced by 30% or 53%, respectively. This suggests that formation of a kissing-loop interaction between kl-TSS transcripts and the 5′89+3U hairpin 5H2 contributes to *trans*-inhibition but is not the sole contributor.

To determine if the ribosome-binding activity of the kl-TSS

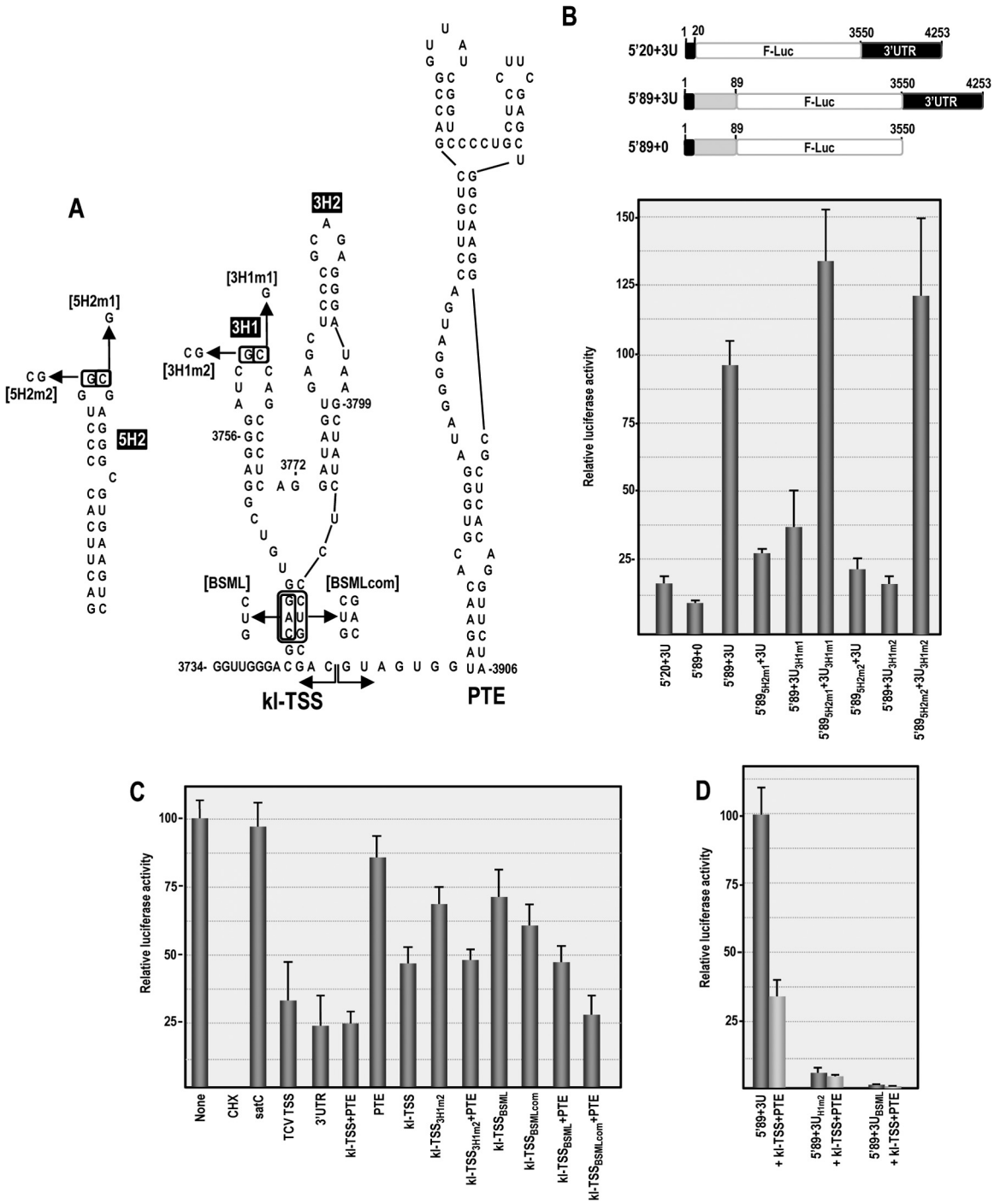

FIG 2 The PEMV kl-TSS competes more efficiently than the PTE in translation of a reporter construct in WGE. (A) Secondary structure of hairpin 5H2 and the kl-TSS and PTE. The boundary between the kl-TSS and PTE fragments is indicated. Locations of mutations, with their names bracketed, are indicated. (B) Relative translation of luciferase reporter transcripts containing the PEMV 5′89 or exact 20-nt 5′UTR and the exact 702-nt 3′UTR in WGE. Constructs used are shown at the top. Mutations were generated in 5′89+3U. White rectangles represent the luciferase ORF, filled rectangles represent the UTR, and gray rectangles represent the coding region. Locations of the mutations are shown in panel A. (C) Translation inhibition assay in WGE. The indicated competitor RNA was added in a 10-fold molar ratio to reaction mixtures containing 5′89+3U. (D) Relative translation of various luciferase reporter transcripts in the presence of the kl-TSS+PTE fragment in WGE. The 5′89+3U$_{3H1m2}$ and 5′89+3U$_{BSML}$ constructs contain the kl-TSS with mutations in 3H1 and the basal stem, respectively. The means and standard deviations for three replicate experiments are shown.

also contributes to *trans*-inhibition, kl-TSS transcripts were generated with mutations disrupting the basal stem (kl-TSS$_{BSML}$) that were previously shown to decrease binding to 80S ribosomes but to not affect the kissing-loop interaction (12). Addition of kl-TSS$_{BSML}$ reduced translation by 28%, and translation inhibition was slightly increased when the basal stem was reformed by compensatory mutations (kl-TSS$_{BSMLcom}$). kl-TSS$_{BSML}$+PTE reduced translation by 52% (compared with 75% for wt tran-

scripts), and the compensatory mutation reforming the basal stem (kl-TSS$_{BSMLcom}$+PTE) restored inhibition to nearly wt levels. The TCV TSS, which binds to 60S ribosomal subunits and 80S ribosomes but does not form any RNA-RNA interaction, also inhibited translation in *trans* (by 67%). Addition of TCV satellite satC (356 nt), which shares a similar 3′ region with TCV but does not bind to ribosomes (23), did not inhibit translation in *trans*. These results suggest that both ribosome-binding and RNA-RNA interaction activities of the kl-TSS contribute to *trans*-inhibition. In addition, these results indicate that the kl-TSS is a stronger inhibitor than the adjacent PTE and that inhibition of translation is enhanced when both 3′CITEs are together.

Since kl-TSS+PTE was inhibitory in *trans*, the elements comprising it likely cannot function as 3′CITEs in *trans*. To confirm this possibility, kl-TSS+PTE transcripts were added in *trans* to translation templates that were unable to engage in the kissing-loop interaction (5′89+3U$_{H1m2}$) in *cis* or to efficiently bind to ribosomes (5′89+3U$_{BSML}$) in *cis* (Fig. 2D). Using a 10-fold molar excess of wt kl-TSS+PTE, no complementation of translation was observed, suggesting that the kl-TSS+PTE 3′CITE module enhances translation in WGE only in *cis*.

PEMV kl-TSS and TCV TSS bind to different sites on 80S ribosomes. 3′CITEs that mimic tRNAs have been found in three viruses. The TSS of the carmovirus TCV and the putative TSS of the closely related *Cardamine chlorotic fleck virus* (CCFV) are structurally very similar and identically positioned near the 3′ ends of their genomes (25). In contrast, the PEMV kl-TSS is located in the central region of its 702-nt 3′UTR, just upstream of the PTE 3′CITE (Fig. 1). In addition to positional differences, the TCV TSS and PEMV kl-TSS differ in their ability to bind to 40S ribosomal subunits and in their capacity to directly engage in a long-distance interaction with a 5′ proximal hairpin. These differences suggested that the TCV TSS and PEMV kl-TSS may have unique modes of action, prompting an investigation into whether the TCV TSS and PEMV kl-TSS bind to ribosomes at similar or different locations. To this end, EMSAs were conducted to determine if the two TSS compete for the same ribosome-binding site. Figure 3A, lane 2, shows the shift in electrophoretic mobility that occurred when labeled kl-TSS bound to purified *Arabidopsis* 80S ribosomes. When 1- to 10-fold cold TCV TSS was included in the reaction mixture, little or no competition for ribosome binding occurred between the two TSS (Fig. 3A, lanes 3 to 6). In contrast, addition of 1- to 10-fold cold kl-TSS led to efficient competition (Fig. 3A, lanes 7 to 10). satC was included as a control and was unable to compete efficiently with kl-TSS binding, as expected (Fig. 3A, lanes 11 to 14). The reverse experiment produced similar results, with cold kl-TSS unable to effectively compete with labeled TCV TSS for ribosome binding, and with cold TCV TSS acting as an effective competitor (Fig. 3B). These results strongly suggest that the PEMV kl-TSS and the TCV TSS bind to different sites in 80S ribosomes.

kl-TSS bound to ribosomes can also engage in the kissing-loop interaction as assayed by in-line RNA structure probing. Since the PEMV kl-TSS engages in an RNA-RNA interaction and binds to ribosomes, an unanswered question with significant implications for the mechanism of kl-TSS translational enhancement is whether binding of the kl-TSS to ribosomes and formation of the kissing loop between kl-TSS hairpin 3H1 and 5′ hairpin 5H2 can occur simultaneously. As a first step to addressing this question, in-line structure probing was used to examine if specific

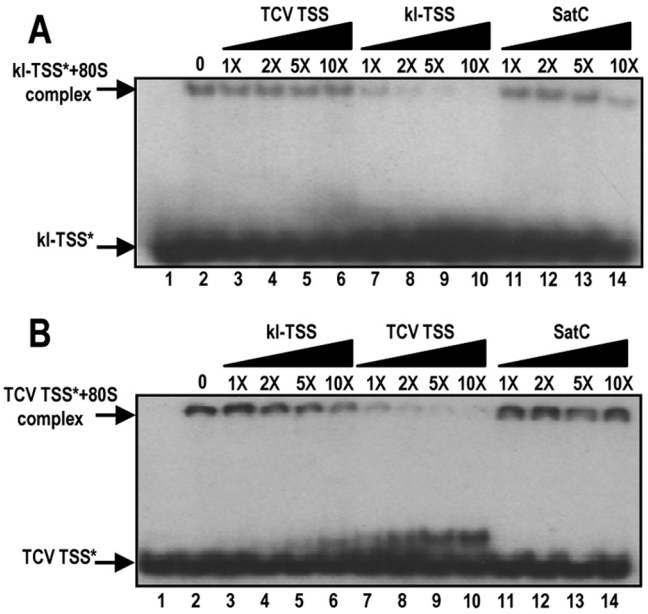

FIG 3 The kl-TSS and TCV TSS do not compete for ribosome binding. The 5′-end-labeled kl-TSS (A) or TCV TSS (B) was combined with *Arabidopsis* 80S ribosomes (lanes 2 to 14) in the absence or presence of an increasing molar excess of unlabeled competitor RNA, as indicated above the lanes. The positions of free labeled RNA and the RNA-ribosome complex are indicated. Asterisks denote labeled RNA. "0" denotes no added competitor RNA. satC is an untranslated satellite RNA of TCV.

structural changes that result from ribosome binding and formation of the kissing-loop interaction can be present at the same time. In-line probing reports on the flexibility of residues, as only flexible residues can adopt the conformation necessary for 2′-hydroxyl-mediated self-cleavage of the nucleic acid backbone (43). When end-labeled RNAs are allowed to self-cleave, the extent of backbone cleavage at a particular residue correlates with the flexibility of that residue. Base pairing with an RNA in *trans*, interaction with a protein in *trans*, or conformational shifts mediated by *trans*-acting factors can significantly reduce cleavages at previously flexible residues (or increase cleavages at previously inflexible residues) (12, 13, 35).

Structural changes due to ribosome binding to the kl-TSS or to 5′89 containing interacting hairpin 5H2 were examined in the presence and absence of the kissing-loop interaction. The flexibility pattern of 5′-end-labeled kl-TSS alone is shown in Fig. 4A, lane 3, and is consistent with the two-hairpin, three-way branched structure that was previously postulated (12). Addition of 40S subunits caused distinctive, reproducible changes in the flexibility of specific residues within the kl-TSS, including a reduction in the flexibility of nearly all residues in the loop of hairpin 3H1, which is the sequence that engages in the kissing-loop interaction (Fig. 4A, lane 4). In addition, residues U3805 and C3806, located within the three-way branch junction region, also lost partial flexibility, and residues A3789 and A3798, located within the terminal and internal loops of 3H2, gained flexibility. Addition of 60S subunits produced similar changes, with the exception that the flexibility of residue A3798 was no longer altered (Fig. 4A, lane 5). In the presence of 80S ribosomes, the basic flexibility patterns seen with 40S and 60S subunits were present, along with some additional differences (Fig. 4A, lane 6). Four residues became more flexible only in

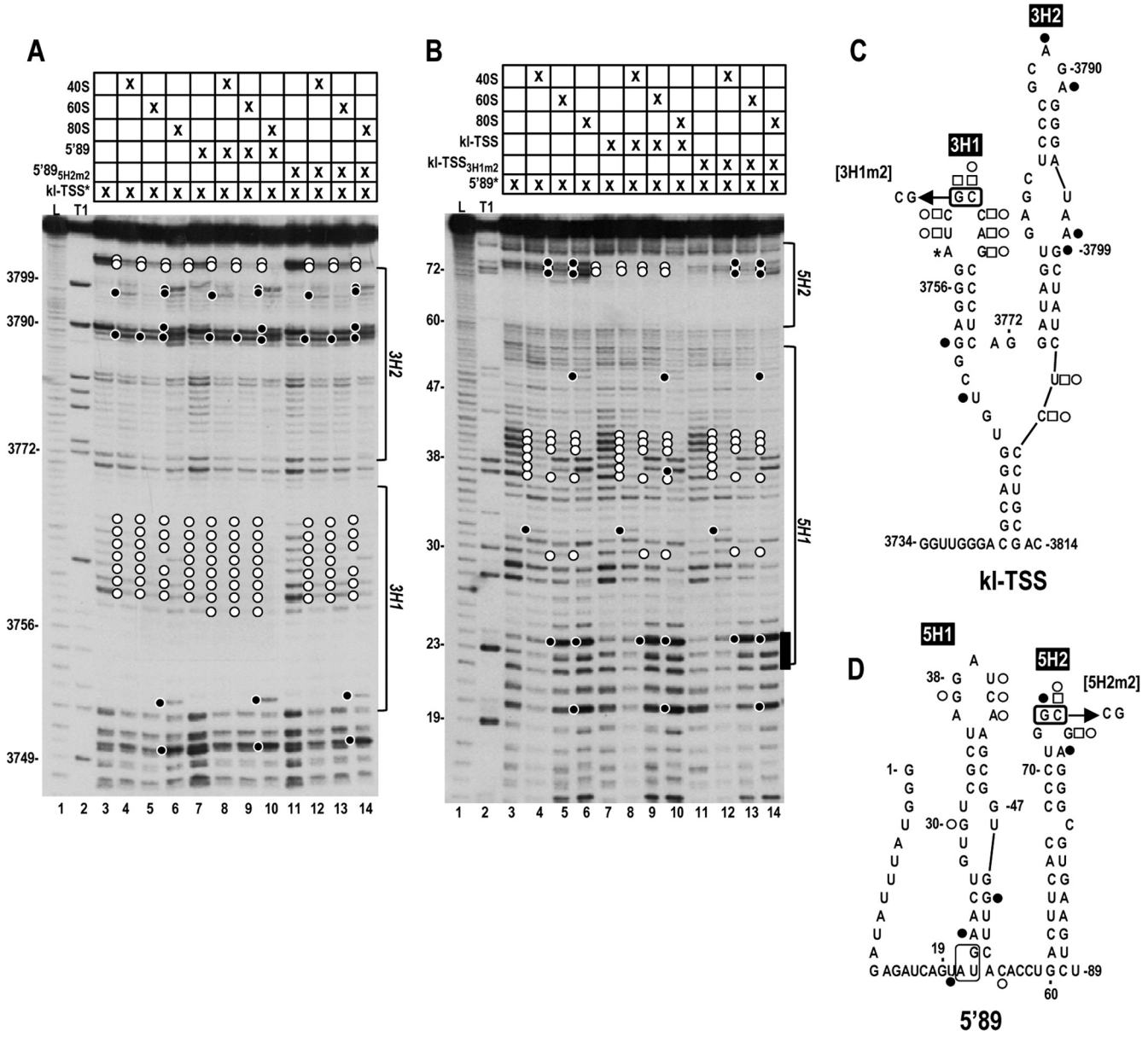

FIG 4 In-line probing of the kl-TSS or 5′89 in the presence or absence of ribosomes and the interacting RNA. (A) In-line probing of 5′-end-labeled kl-TSS in the presence and absence of cold 5′89 and *Arabidopsis* 40S/60S subunits and 80S ribosomes. The intensities of the bands in lanes 3 to 14 are proportional to the flexibility of the residues. The asterisk denotes the radioactive fragment. L, alkaline-generated ladder; T1, partial RNase T1 digest of denatured kl-TSS for locating guanosine residues. Open and filled circles denote residues with consistently reduced and enhanced flexibility, respectively, in the presence of 5′89 and/or ribosomes. Locations of the hairpins are indicated to the right of the panel. (B) In-line probing of 5′-end-labeled 5′89 in the presence and absence of cold kl-TSS and *Arabidopsis* 40S/60S subunits and 80S ribosomes. (C) Locations of residues with flexibility alterations in the kl-TSS in the presence of 80S ribosomes (circles), 5′89 (squares), or 5′89+80S only (*). Open symbols and filled symbols denote residues with consistently reduced and enhanced flexibility, respectively. The locations of mutations in kl-TSS$_{3H1m2}$ are indicated. (D) Locations of residues with flexibility alterations in 5′89 in the presence of 80S ribosomes (circles) and kl-TSS (squares). The p33 initiation codon is boxed. The locations of mutations in 5′89$_{5H2m2}$ are indicated.

the presence of 80S ribosomes (U3750, G3753, A3791, and G3799), and residue G3761 in the 3H1 loop no longer had reduced flexibility.

As previously demonstrated (12), when kl-TSS hairpin 3H1 is engaged in the kissing-loop interaction with 5′89 hairpin 5H2, nearly all residues in the loop of 3H1 lose flexibility, although only 6 of the 8 are postulated to form Watson-Crick base pairs with the 5H2 terminal loop (Fig. 1). In addition, residues U3805 and C3806 in the three-way branch junction region also lose partial flexibility (Fig. 4A, lane 7). When both ribosomes and 5′89 were added to the kl-TSS, residue flexibility changes were basically additive (Fig. 4A, lanes 8 to 10, and C). For example, U3805 and C3806, which lost partial flexibility in the presence of ribosomes or 5′89, were not subject to detectable cleavage when both ribosomes and 5′89 were present. Additionally, nearly all residues with enhanced flexibility in the presence of ribosomes and ribosomal subunits retained their flexibility profiles. G3761, which remained partially flexible in the presence of 80S ribosomes but produced no

cleavage in the presence of 5′89, was no longer flexible in the presence of both 80S ribosomes and 5′89. In addition, one new residue (G3758) in the 3H1 terminal loop lost flexibility (Fig. 4C). When $5'89_{5H2m2}$, which contains a 2-nt alteration in hairpin 5H2 (Fig. 4D), was used in the assay, the cleavage profile was very similar to that of the kl-TSS alone (Fig. 4A, lane 11), indicating that the RNA-RNA interaction no longer formed, as previously found (12). When ribosomes and ribosomal subunits were added to the kl-TSS and $5'89_{5H2m2}$, the cleavage pattern of the kl-TSS was very similar to the pattern obtained when the kl-TSS was assayed in the absence of any added fragment (Fig. 4A, compare lanes 4 to 6 with lanes 12 to 14).

The experiment was repeated using 5′-end-labeled 5′89, whose cleavage pattern is shown in Fig. 4B, lane 3. Addition of 40S subunits reduced the flexibility of all residues in the loop of hairpin 5H1, except for residue A36 (Fig. 4B, lane 4). In addition, residue G30 in the asymmetric bulge loop of 5H1 exhibited reduced flexibility, and C32 became more flexible. Addition of 60S subunits or 80S ribosomes produced similar patterns that differed substantially from the 40S subunit-generated pattern, with residues throughout the fragment gaining or losing flexibility (Fig. 4B, lanes 5 and 6). Interestingly, residues within the apical loop of 5H2 that participate in the RNA-RNA interaction exhibited substantial flexibility changes, with C74 and G75 losing flexibility and G73 and A76 gaining flexibility.

When the kl-TSS was added to labeled 5′89, only the flexibility of residues C74 and G75, located in the apical loop of 5H2, was substantially reduced, as these residues pair with kl-TSS hairpin 3H1 (Fig. 4B, lane 7) (12). When both ribosomes and the kl-TSS were added, the cleavage pattern in the loop of 5H2 reflected the RNA-RNA interaction pattern (complete loss of flexibility), whereas the pattern elsewhere in 5′89 reflected the ribosome pattern (Fig. 4B, lanes 8 to 10, and D). Addition of kl-TSS_{3H1m2} along with ribosomes or ribosomal subunits resulted in cleavage patterns that were very similar to those obtained in the absence of the added fragment (Fig. 4B, compare lanes 4 to 6 with lanes 12 to 14). Together, these results suggest that the kissing-loop interaction between the kl-TSS and 5′89 does not obviate ribosome binding to the fragments.

The kl-TSS bound to ribosomes engages in the kissing-loop interaction as assayed by hSHAPE. Selective 2′-hydroxyl acylation analyzed by primer extension (SHAPE) probes RNA structure by measuring the sensitivity of residues to compounds such as 1M7, which reacts with 2′-hydroxyl groups of flexible nucleotides (44) and impedes the progress of complementary strand synthesis by reverse transcriptase. High-throughput SHAPE (hSHAPE) uses fluorescently labeled oligonucleotide primers to perform the reverse transcription-mediated primer extension, allowing products to be separated by capillary electrophoresis and data to be analyzed in a quantitative fashion using ShapeFinder software (33, 45, 46).

Our reasoning for conducting hSHAPE of rRNAs in the presence of the kl-TSS and kl-TSS+5′89 was as follows. If the kl-TSS binds to the same ribosome site when alone and when base paired with hairpin 5H2, and if the structure of the kl-TSS is not substantially altered in complex with 5H2, then the kl-TSS and kl-TSS+5′89 should produce mainly similar changes to the SHAPE signature pattern of the rRNAs within the ribosome (i.e., the kissing-loop interaction with 5′89 should not prevent binding of the kl-TSS to a particular site in the ribosome and the concomitant structural changes that occur). However, the flexibility profiles for the kl-TSS and kl-TSS+5′89 should not be identical, as differences would be expected that reflect the presence of a 12-bp helix (5H2) joined to the kl-TSS and any structural changes in the kl-TSS caused by formation of the kissing loop.

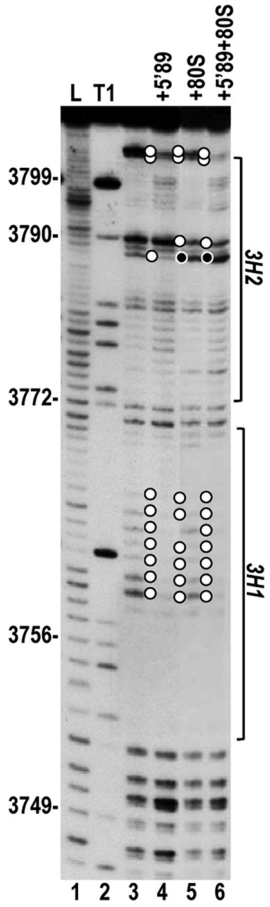

FIG 5 In-line probing of the kl-TSS in the presence of yeast ribosomes and 5′89. 5′-End-labeled kl-TSS in the presence and absence of cold 5′89 and yeast 80S ribosomes was subjected to in-line probing. The intensities of the bands in lanes 3 to 6 are proportional to the flexibility of the residues. L, alkaline-generated ladder; T1, partial RNase T1 digest of denatured kl-TSS for locating guanosine residues. Open and filled circles denote residues with reduced and enhanced flexibility, respectively, in the presence of 5′89 and/or 80S ribosomes. Locations of the hairpins are indicated to the right of the panel.

Yeast 80S ribosomes were used for this analysis because hSHAPE flexibility profiles are available for salt-washed yeast 80S rRNAs (33), which were obtained using a set of 20 fluorescently labeled primers. The kl-TSS binds to yeast 80S ribosomes with a K_d of 0.29 μM, which is lower than the K_d for binding to *Arabidopsis* ribosomes (0.52 μM) (12). To evaluate if yeast and *Arabidopsis* 80S ribosomes interact in a similar fashion with the kl-TSS, in-line probing was conducted for the kl-TSS bound to yeast 80S ribosomes in the presence and absence of 5′89 (Fig. 5). Although the flexibility profiles for the kl-TSS bound to *Arabidopsis* or yeast 80S ribosomes were not identical, the major ribosome-mediated structural alterations were all present. These included the reduced flexibility of most residues in the loop of 3H1 and of the three-way junction residues U3805 and C3806, as well as altered flexibility in the terminal loop of 3H2. In the presence of 5′89, the flexibility

alterations were additive, as previously found for *Arabidopsis* 80S ribosomes. These results suggest that *Arabidopsis* and yeast ribosomes interact with the kl-TSS in a similar fashion.

The reactivities of rRNA residues to 1M7 in the presence of the kl-TSS were compared to those of rRNA in salt-washed ribosomes, generating a profile of reactivity changes due to the presence of the kl-TSS (Fig. 6A and B, left structures, and C, top structure). The changes in reactivity of rRNA residues were grouped into nine levels and color coded to represent the degree of flexibility change due to the presence of the kl-TSS. Each color change represents a statistically significant change in base reactivity. For example, black or 0 denotes changes in reactivity that are less than a trace's median value, yellow or 1 represents increases in reactivity between the median and the mean, light orange or 2 is used for increases in reactivity between the mean and the 1st standard deviation, dark orange or 3 designates increases in reactivity between the 1st and 2nd standard deviations, and red or 4 indicates increases in reactivity above the 2nd standard deviation. Similarly, decreased reactivities relative to those of empty ribosomes are denoted by progressively cooler colors.

Seven rRNA hairpins contained substantial chemical reactivity changes in the presence of the kl-TSS relative to empty ribosomes (Fig. 6A, left structure): H82, H69, and H89 in the 25S rRNA and h10, h33, h42/43, and the upper portion of h44 in the 18S rRNA. These structures, shown in green in Fig. 6D, are located mainly on the face of the ribosome that is visible when viewed from the mRNA tunnel closest to the A site. H82 is adjacent to H80, the "P loop" that interacts with the 3′ end of the peptidyl-tRNA; H89 lines one side of the aminoacyl-tRNA accommodation corridor and interacts with the acceptor stem of tRNAs entering the A site (47); and H69, which is located between the small and large ribosomal subunits, makes extensive contacts with A-site tRNA (48). The small subunit of h44 (upper portion) also interacts with A-site tRNAs in the decoding center (49). Although determining the position of the kl-TSS in the ribosome was not a goal of this study, these results suggest that the kl-TSS might bind in or near the ribosome A site.

kl-TSS+5′89 was subjected to a similar hSHAPE analysis. The RNA fragments were preincubated under conditions that achieve approximately 90% formation of the kissing-loop interaction (1:3 ratio of kl-TSS to 5′89) as assayed by EMSA (12). The rRNA helices that exhibited major flexibility changes when the kl-TSS was assayed alone produced similar flexibility changes with kl-TSS+5′89 (Fig. 6A, middle structures). The similar flexibility profiles for these rRNA hairpins strongly suggest that the kl-TSS alone and paired with 5′89 hairpin 5H2 bind to similar sites in 80S ribosomes.

On the side of the A-site accommodation corridor that lies opposite H89 are helices H90, H91, and H92 (50). The presence of the kl-TSS resulted in a strong decrease in base reactivity for residue U2865, located in the 3-way junction connecting these helices (Fig. 6C). Upon addition of 5′89, U2865 and the 5′-adjacent residue G2864 exhibited +4 increases in reactivity (Fig. 6C, bottom structure). In addition, three helices (H50, H61, and ES39) exhibited major structural changes only in the presence of kl-TSS+5′89. Three of six residues in the terminal loop of 25S rRNA H50 became strongly reactive, as did one side of the H50 stem (Fig. 6B, compare left and middle structures). Residues on both sides of ES39 and one side of H61 also became highly reactive in the presence of kl-TSS+5′89 only. These perturbations in rRNA structure when the kl-TSS is linked to 5′89 suggest that there are more complex binding interactions than are currently understood. The locations of H50, H61, and ES39 in the ribosome are shown in Fig. 6E (in blue). H50 and H61 are adjacent to and located on one side of the peptide exit channel. ES39 is located on the opposite side but is not adjacent to the exit channel. Since these helices are distal to the A-site location of most of the helices with major flexibility changes due to the kl-TSS, it is currently unknown why these helices are substantially altered in the presence of kl-TSS+5′89.

To determine if residue flexibility differences between kl-TSS-bound ribosomes and kl-TSS+5′89-bound ribosomes were due to the kissing loop between the kl-TSS and 5′89 hairpin 5H2, and not the 5′89 fragment alone, hSHAPE was repeated using kl-TSS+5′89_{5H2m2}, which contains two base changes in the interacting sequence. Flexibility profiles for H50, ES39, and H61 were now more similar to those found in the presence of the kl-TSS alone (Fig. 6A and B, right structures), suggesting that the majority of flexibility changes were not due to an interaction with just the 5′89 fragment. The hairpins displaying similar flexibility changes with the kl-TSS alone and kl-TSS+5′89 also had similar flexibility profiles in the presence of kl-TSS+5′89_{5H2m2} (Fig. 6A). Flexibility profiles for G2864 and U2865 at the base of H91 were also similar to those found for the kl-TSS alone (not shown). Together, these results suggest that the altered flexibility profiles exclusive to kl-TSS+5′89 resulted from the 12-bp hairpin paired with the kl-TSS, not from 5′89 alone.

Dissociation constants are similar for kl-TSS bound to ribosomes in the presence and absence of 5′89. To determine if the ribosome dissociation constant for the kl-TSS is affected when the kl-TSS engages in the RNA-RNA interaction, filter binding assays were conducted for labeled kl-TSS and 80S *Arabidopsis* ribosomes in the presence and absence of precomplexed 5′89 and 5′89_{5H2m2}. A 3-fold molar excess of unlabeled 5′89 or 5′89_{5H2m2} was used in this assay, which for 5′89 produces ~90% interacting molecules (12). The K_d for PEMV kl-TSS binding to salt-washed *Arabidopsis* 80S ribosomes was previously determined to be 0.52 μM (12). For the current study, the K_d for kl-TSS binding to salt-washed *Arabidopsis* 80S ribosomes was 0.61 μM (Fig. 7A), similar to our previously published value. When the kl-TSS was first complexed with 5′89, the K_d was essentially unaffected (0.58 μM) (Fig. 7B). The K_d was also unaffected when the kl-TSS was in the presence of 5′89_{5H2m2}, which cannot form the RNA-RNA interaction (K_d = 0.55 μM) (Fig. 7C). These results suggest that formation of the kissing-loop interaction between the kl-TSS and 5′89 hairpin 5H2 does not affect the efficiency of kl-TSS binding to ribosomes. Therefore, these results support the conclusions of the in-line structure probing and hSHAPE studies, i.e., that RNA-RNA interaction and ribosome binding are compatible activities for the kl-TSS.

The kl-TSS maintains a T shape when engaged in the highly stable kissing-loop interaction. Previous modeling of the kl-TSS 3-D structure by use of RNA2D3D (36) predicted a T-shaped structure for the kl-TSS (12). The hSHAPE and filter binding results suggest that when the kl-TSS is engaged in the kissing-loop interaction, the T shape must be maintained to support similar binding properties with ribosomes. To determine (i) if the structure of the kl-TSS is affected by docking to 5H2 and (ii) the stability of the kissing-loop interaction, MD simulations were conducted for the model kl-TSS/5H2 docked structure and kl-TSS alone. An all-atom root mean square deviation (RMSD) plot mea-

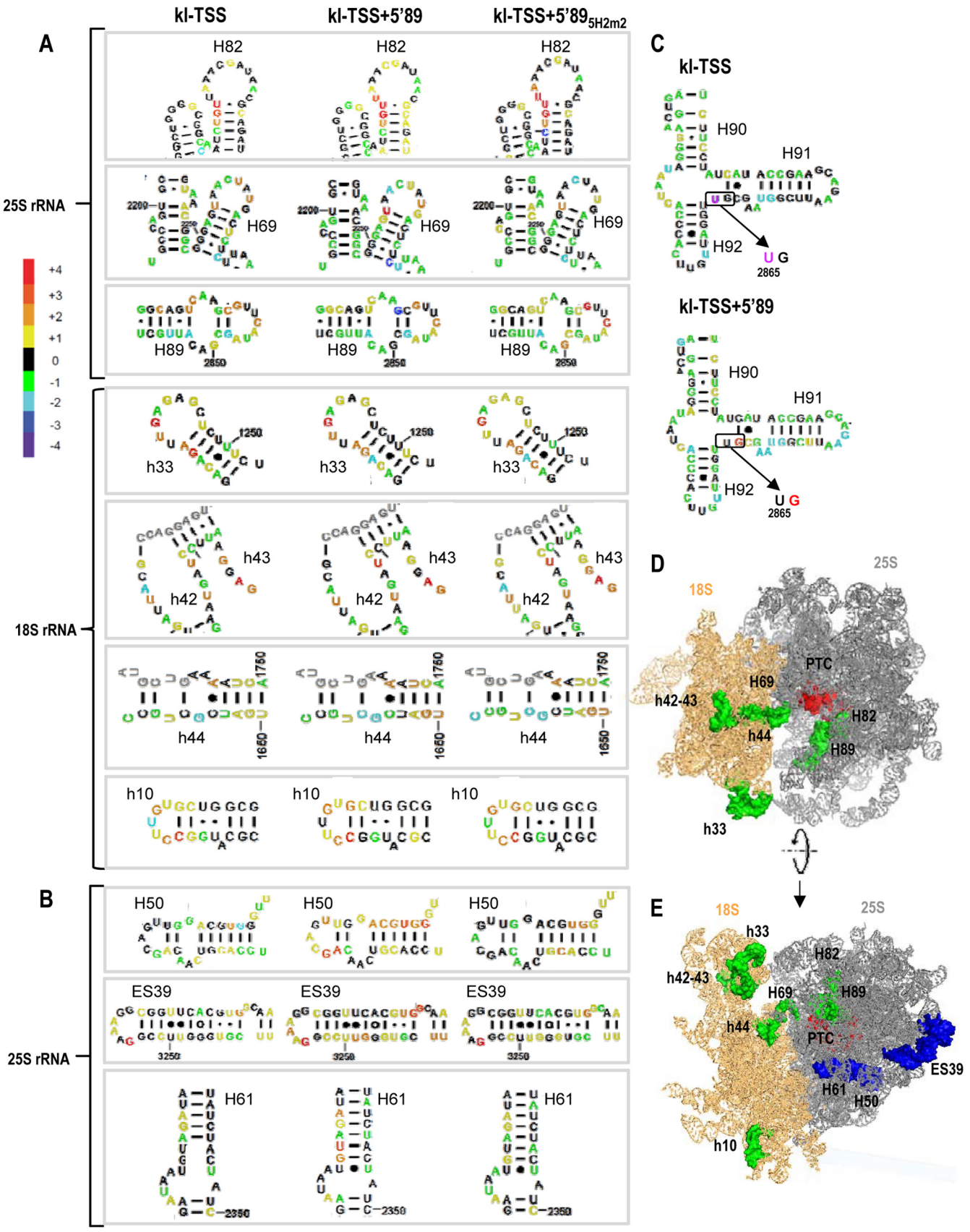

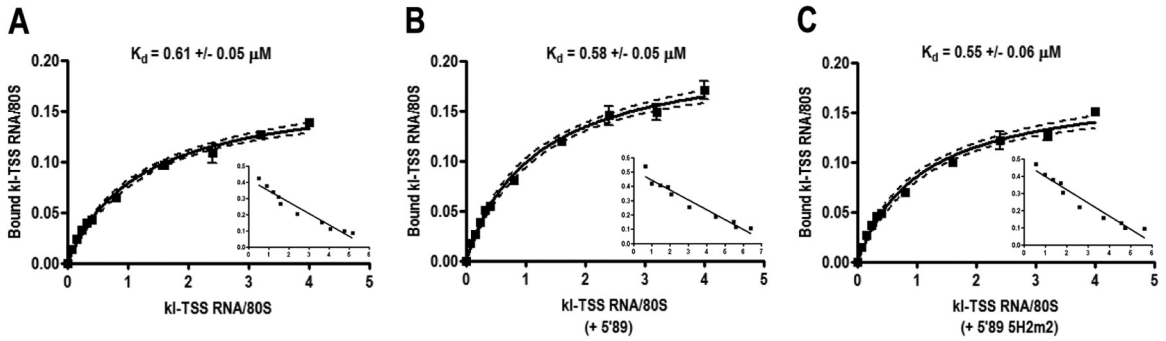

FIG 7 Dissociation constants for the kl-TSS bound to ribosomes in the presence and absence of 5′89 as assayed by filter binding. Two to 60 pmol of 5′-end-labeled kl-TSS was incubated with 15 pmol of salt-washed *Arabidopsis* 80S ribosomes, and bound RNA was detected following filtration. (A) kl-TSS only. (B) kl-TSS preincubated with a 3-fold molar excess of unlabeled 5′89. (C) kl-TSS preincubated with a 3-fold molar excess of unlabeled 5′89 with a two-base alteration in the loop of the interacting hairpin 5H2 ($5'89_{5H2m2}$). The saturation binding curves are shown together with Scatchard plots (insets). K_d values were calculated from three independent experiments. Error bars represent standard errors.

sured against the average structure for the full trajectory (3,221 atoms; 58-ns MD trajectory) of the kl-TSS/5H2 docked structure has a mean value of 4.9 ± 1.2 Å (Fig. 8), illustrating the overall stability of the model. The average 3-D structure of the kl-TSS/5H2 docked model (Fig. 8B) shows that the initial kl-TSS T shape (Fig. 8A, right panel) is retained in the MD simulation. The overall T shape is also clearly visible in the overlay of this structure in two possible orientations with $tRNA_{Phe}$ (Fig. 9B; shown even more strikingly in Fig. 9D). RMSDs of individual stems (not shown, because the graphs overlap) were also low, with 3H2 contributing most of the distortions caused by the large asymmetric internal loop. Collective, scissor-like motions of the 3H1 and 3H2 arms of the kl-TSS toward and away from each other were the most visible slow conformation changes. A very similar average MD structure (all-atom RMSD of 6.9 Å) was also obtained from an MD run of 97 ns for the kl-TSS alone (Fig. 8B, bottom structure). The reduced mean value of the RMSD for 3H1 in kl-TSS/5H2 compared to the RMSD of 3H1 in the kl-TSS alone indicates that while the kl-TSS retains its shape, the 3H1-5H2 interaction stabilizes 3H1.

The red RMSD plot shown in Fig. 8C was calculated for all nucleotide atoms involved in the kissing-loop interaction up to the base pairs closing the two hairpin loops (C70-G77 in 5H2 and G3757-C3766 in 3H1). The low mean RMSD value of 0.9 ± 0.2 Å measured against the average structure indicates a structurally stable kissing-loop interaction. The hydrogen bond occupancy analysis for the same nucleotides shows that 6 bp form stable bonds (93 to 100% occupancy for the A76-U3759, G75-C3760, C74-G3761, G73-C3762, G72-C3763, and U71-A3764 pairs, with the majority of bonds being in the 99 to 100% occupancy range). Thus, the initial (after minimization) approximate kissing-loop model (Fig. 8A, right panel) was transformed in the dynamics simulation into a very stable interaction (see the adjustments to the 5H2 structure in the average model [Fig. 8B, top structure]). The stem-closing base pairs (C70-G77 in 5H2 and G3757-C3766 in 3H1) are also extremely stable (99 to 100% occupancy). Overall, the MD results indicate that the T-shaped conformation of the kl-TSS is maintained when the kl-TSS is docked with 5H2 and that the kissing-loop complex between the kl-TSS and 5H2 is stable. Similar results supporting the above conclusions were obtained using the structure "B" model (12) for the kl-TSS and kl-TSS/5H2 (results not shown), even though the initial kl-TSS conformation is a distinct alternative to structure "A."

DISCUSSION

Significant differences exist between the TCV TSS and PEMV kl-TSS. A wide range of plus-strand RNA viruses use 3′CITEs for efficient translation of their encoded proteins (11, 51). Among various types of 3′CITEs, those that mimic tRNAs and possess direct ribosome-binding ability have been identified only in the carmovirus TCV, its close relative CCFV, and the umbravirus PEMV. The TCV TSS and PEMV kl-TSS have different structural, positional, and functional properties, suggesting that TSS-type 3′CITEs may not have a single mode of action. For example, (i) the TCV TSS is composed of three hairpins and two pseudoknots (25), whereas the PEMV kl-TSS contains a two-hairpin, three-way junction structure (12); (ii) the TCV TSS is located proximal to the 3′ end of the genome and overlaps elements involved in transcription of complementary strands (25, 35), whereas the PEMV kl-TSS is positioned near the central region of its much longer 3′UTR and is adjacent to a second 3′CITE, the eIF4E-binding PTE (12); (iii) the TCV TSS does not participate in any discernible long-distance interaction, whereas the PEMV kl-TSS engages in a crit-

FIG 6 Alteration of the flexibility profile of rRNAs in yeast 80S ribosomes in the presence of the kl-TSS, kl-TSS+5′89, and a kl-TSS+5′89 variant that cannot participate in the RNA-RNA interaction. (A) Helices with major structural alterations in 25S and 18S rRNAs in the presence of bound kl-TSS (left), kl-TSS+5′89 (middle), and kl-TSS+$5'89_{5H2m1}$ (right). The flexibility profiles were generated by subtracting the flexibility values for salt-washed ribosomes from the flexibility values of residues for ribosomes in the presence of the added transcripts. The color code is shown at left. Each color change represents a standard deviation change in flexibility, with the "warm" colors (e.g., red, orange, and yellow) indicating more flexible residues and the "cool" colors (green, blue, and purple) denoting less flexible residues. Gray residues could not be evaluated. (B) Three helices that exhibited major structural changes in the presence of kl-TSS+5′89 only. (C) Three helices that line the A-site accommodation corridor. The purple uracil residue denotes a substantial decrease in flexibility at this position in the presence of the kl-TSS. (D) Locations of altered helices in 80S ribosomes. The 60S subunit is colored gray, and the 40S subunit is colored tan. Helices with major structural alterations are shown in green. The peptidyltransferase center (PTC) is shown in red. The view is looking into the mRNA tunnel nearest the A site. (E) Different view of 80S ribosomes to show the locations of helices (in blue) that have major structural changes with kl-TSS+5′89 only.

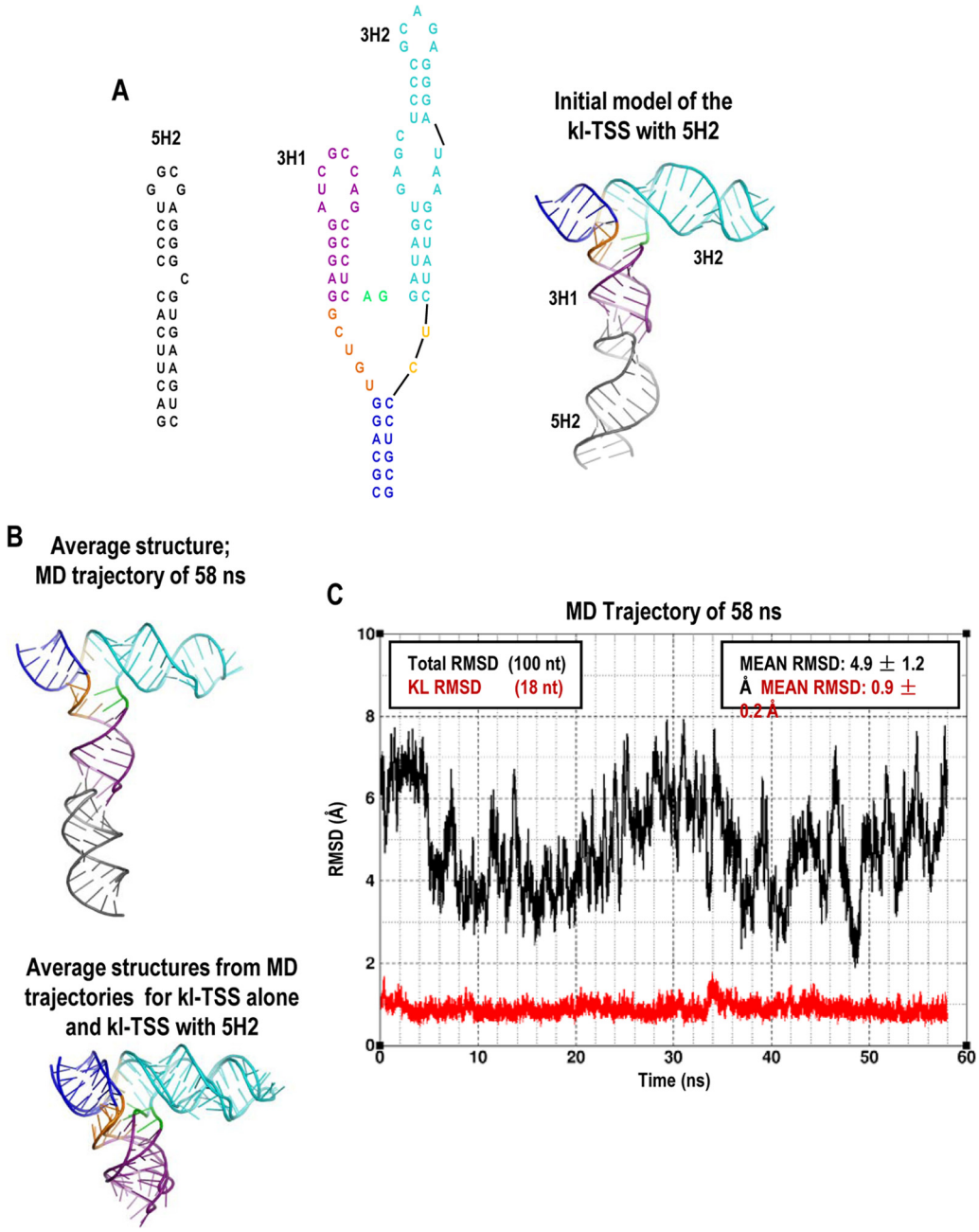

FIG 8 Molecular dynamics simulation of the kl-TSS/5H2 complex. (A) (Left) Secondary structure of the 5′ hairpin 5H2. (Center) kl-TSS color coded with the model to the right. (Right) Energy-minimized 3-D model of the kl-TSS docked with 5H2, built using RNA2D3D (36), based on the previously published kl-TSS model (structure A in reference 12). (B) (Top) Average 3-D structure based on a 58-ns MD trajectory. (Bottom) Overlay of the average kl-TSS structures from two independent MD trajectories for the kl-TSS/5H2 complex (58 ns) and the kl-TSS alone (97 ns). The all-atom RMSD (2,288 atoms) between the two kl-TSS structures is 6.9 Å. (C) RMSD plot for the 58-ns MD trajectory for the model shown in panel A. RMSD values plotted in black were calculated for all 3,221 nucleic acid atoms (i.e., excluding the solvent and ions) relative to the minimized average MD structure shown in panel B. RMSD values plotted in red are the values calculated for all atoms of the 18 nt involved in and flanking the kissing-loop interaction between 5H2 (nucleotides C70 to G77) and 3H1 (nucleotides G3757 to C3766). The low mean RMSD and standard deviation of the kissing-loop nucleotide subset indicate the stability of this interaction, which is in good agreement with the measured stability of the hydrogen bonds involved (see the text for further details).

ical long-distance interaction with coding region hairpin 5H2 (12, 52); and (iv) the TCV TSS binds to 60S subunits and 80S ribosomes and the PEMV kl-TSS binds to both 40S and 60S ribosomal subunits and 80S ribosomes (12, 23).

The TCV TSS competes with a P-site-located tRNA for binding to 80S ribosomes (52), and this localization was recently confirmed by cryo-electron microscopy (cryo-EM) (J. Pallesen, J. Leshin, J. Frank, J. D. Dinman, and A. E. Simon, unpublished data). As shown in Fig. 3, the PEMV kl-TSS does not compete with the TCV TSS for ribosome binding, suggesting that the kl-TSS occupies a site other than the P site in the ribosome. In support of this conclusion, we recently found that the hSHAPE signature for

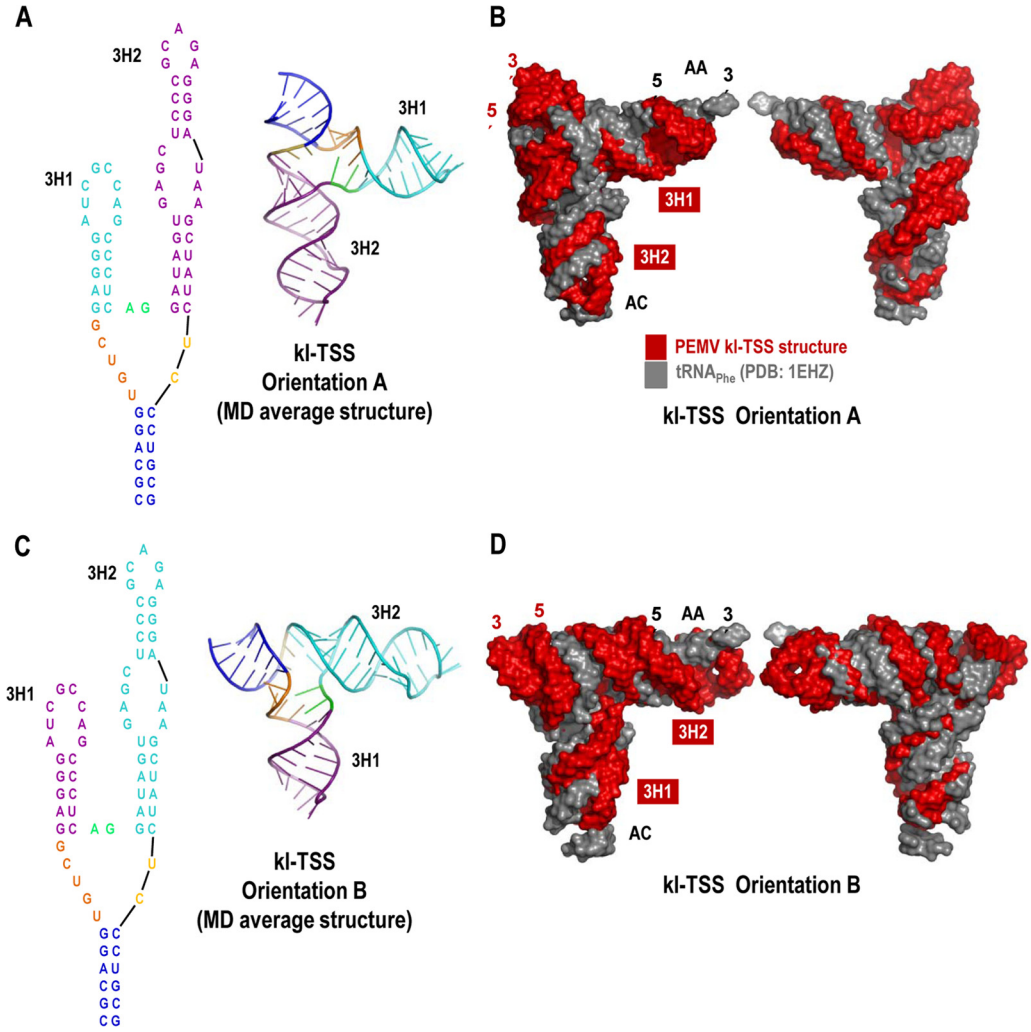

FIG 9 Two possible orientations of the kl-TSS with respect to canonical tRNAs. (A) (Left) Secondary structure of the kl-TSS, with hairpin 3H1 in cyan and hairpin 3H2 in purple. (Right) 3-D structure (orientation A) of the kl-TSS model based on the average structure from the MD simulation for the kl-TSS/5H2 docked structure illustrated in Fig. 8B. This orientation places 3H1 (cyan) in the position of the amino acid acceptor stem and 3H2 (purple) mimicking the anticodon stem. (B) Overlapping of the kl-TSS in orientation A (red) with phenylalanine tRNA ($tRNA_{Phe}$) (Protein Data Bank [PDB] code 1EHZ) (gray). AC, anticodon stem; AA, amino acid acceptor stem. (C) (Left) Similar to panel A (left), except that hairpin 3H1 is in purple and hairpin 3H2 is in cyan. (Right) 3-D structure (orientation B) of the kl-TSS with 3H1 (purple) in the position of the anticodon stem and 3H2 (cyan) mimicking the amino acid acceptor stem. (D) Alignment of the 3-D structure of the kl-TSS in orientation B (red) with $tRNA_{Phe}$ (gray).

rRNAs in TCV TSS-bound 80S ribosomes is similar to that found for P-site-binding tRNAs and markedly different from the pattern found for the kl-TSS (J. Leshin, J. D. Dinman, and A. E. Simon, unpublished data). Different ribosome-binding sites, combined with the aforementioned positional, structural, and functional differences, suggest that tRNA mimics may have evolved unique features to achieve efficient translational enhancement in various viral genome contexts.

The kl-TSS can simultaneously bind to ribosomes and engage in its RNA-RNA interaction with the 5′ hairpin 5H2. A significant unanswered question is how the TSS delivers bound ribosomes or ribosomal subunits to the 5′ end of the viral genome. Although it has been proposed that 3′CITEs bind simultaneously to translation factors and the 5′ end (53, 54), this has been shown experimentally only for the I-shaped 3′CITE of *Maize necrotic streak virus* (14). For PEMV, it is not obvious that a ribosome would be able to accommodate the kl-TSS, the viral RNA emanating 5′ and 3′ of the kl-TSS, and a 12-bp hairpin (5H2) docked with kl-TSS hairpin 3H1. Thus, to begin deciphering the mechanism of kl-TSS function, it was important to ascertain if ribosome-binding and long-distance interaction activities are compatible. Using in-line probing to detect the pattern of flexible residues in the kl-TSS or 5′89 due to the presence of the interacting RNA and ribosomes/ribosomal subunits, we found that the flexibility profile was a combination of the patterns found when the kl-TSS was engaged only in the RNA-RNA interaction or only in ribosome binding (Fig. 4). Since the intensities of cleavage products in the presence of both 5′89 and ribosomes were comparable or greater to those present when the kl-TSS was bound only to 5′89 or ribosomes, the most likely interpretation of these results is that both kl-TSS activities were occurring simultaneously. If the activities were not compatible, the expectation would have been that only

~10% of the kl-TSS not forming the kissing-loop interaction would bind ribosomes, producing a much-reduced ribosome flexibility pattern, which was not found. Interestingly, this assay also established that binding of 40S or 60S subunits to the kl-TSS reduced the flexibility of most residues in the loop of hairpin 3H1, which are the same residues that engage in the RNA-RNA interaction (Fig. 4A, lanes 4 and 5). The reduced flexibility of 3H1 residues is likely not due to a direct RNA-RNA interaction with rRNA residues, since the 40S and 60S subunits contain different rRNAs, but may be caused by restrictions imposed by subunit binding. One intriguing possibility is that the bound ribosome freezes 3H1 loop residues in a conformation that supports more efficient base pairing with the partner sequence, which might enhance the rate of ribosome recycling.

Constraints in the flexibility of kl-TSS 3H1 loop residues that occur when these residues are engaged in the kissing-loop interaction were previously found to be coupled to reduced flexibility in junction residues U3805 and C3806 (12) (Fig. 4A, lane 7). As shown in Fig. 4A, lanes 4 to 6, these two nucleotides also lose flexibility when 3H1 loop residues are constrained due to ribosome binding. The flexibility of U3805-C3806 was further reduced when the kl-TSS was both engaged in the RNA-RNA interaction and bound to ribosomes (Fig. 4A, lanes 8 to 10), suggesting an additive effect of the two activities.

Fragment 5′89 exhibited specific changes in residue flexibility in the presence of 40S subunits, with very different changes in the presence of 60S subunits or 80S ribosomes (Fig. 4B). It is currently not known how the ribosome-bound structural changes in 5′89 reflect specific binding sites for the ribosome or ribosomal subunits. As found for the kl-TSS, the 5′89 flexibility pattern due to ribosome binding was maintained when the RNA was engaged in the RNA-RNA interaction, supporting the interpretation that the two activities are not mutually exclusive. Binding of 40S subunits led to a loss of residue flexibility throughout the loop of hairpin 5H1, which might indicate an interaction with a complementary sequence in the 18S rRNA. A search of the *Arabidopsis* 18S rRNA revealed the sequence 1253-5′-CUUGAUUCUA, which is perfectly complementary with the 5H1 terminal loop (5′-UAGGAUCAAG). This 18S rRNA sequence is located adjacent to H33, one of the helices substantially altered by hSHAPE when 80S ribosomes are bound by the kl-TSS (Fig. 6A). Binding of 5′89 to 60S subunits and 80S ribosomes also resulted in striking changes in the flexibility of hairpin 5H2's terminal loop, the sequence that base pairs with kl-TSS hairpin 3H1. This flexibility change in 5H2 may reflect induction of a conformation that is more conducive to forming the kissing-loop interaction, as suggested above based on similar findings for the kl-TSS.

Many of the most significant changes in the hSHAPE flexibility profiles of 18S and 25S rRNAs within 80S ribosomes were similar in the presence of kl-TSS, kl-TSS+5′89, and kl-TSS+5′89$_{5H2m2}$ (Fig. 6A), suggesting that the kl-TSS is accommodated in similar locations within the ribosomes in the absence or presence of the interacting fragment. Three helices (H50, H61, and ES39) and two residues in the three-way junction linking H90, H91, and H92 (U2865 and G2864) exhibited major changes in their flexibility profiles only in the presence of kl-TSS+5′89, e.g., when the kissing-loop interaction formed (Fig. 6B and C). This finding suggests that the kissing-loop interaction does affect, to some extent, the accommodation of the kl-TSS in the ribosome. Interestingly, helices H50 and H61 are adjacent to and at the base of the peptide exit channel (Fig. 6B). Since the peptide exit channel is too narrow to accommodate an RNA double-stranded helix, the reason that these helices are disrupted remains obscure.

Orientation of the kl-TSS with respect to a canonical tRNA. Two of the three 25S rRNA helices (H69 and H89) and one of the four 18S rRNA helices (h44) exhibiting major structural changes in the presence of the kl-TSS directly contact A-site-binding tRNAs. Significant flexibility changes were found in the terminal loop of large-subunit helix H69, which participates in the B2a intersubunit bridge and makes extensive contacts with A-site tRNA and polypeptide tRNA mimics that enter the A site, such as release factors and ribosome recycling factor (55–57). H89, which lines the aminoacyl-tRNA accommodation corridor, also exhibits major flexibility changes in the presence of the kl-TSS, as does the junction region of the three helices (H90, H91, and H92) that line the other side of the accommodation corridor. In the small subunit, the upper portion of h44 interacts with A-site tRNAs in the decoding center. Since the kl-TSS does not compete with the TCV TSS for P-site binding, these results are suggestive that the kl-TSS might bind in or near the ribosome A site.

The RNA2D3D updated model of the kl-TSS (Fig. 8A) converged to a T-shaped structure in the kl-TSS/5H2 MD simulations (Fig. 8B). This result is additionally supported by an alternative model (structure "B" model in reference 12) that converges to the common kl-TSS shape. Two possible orientations for the averaged MD structure of the kl-TSS relative to a canonical tRNA are shown in Fig. 9. In orientation A (the orientation previously published [12]), hairpin 3H1, which participates in the long-distance RNA-RNA interaction, was proposed to mimic the amino acid acceptor arm of a tRNA (Fig. 9A and B). Based on our finding that kl-TSS alone and kl-TSS bound to 5H2 are accommodated in the same approximate location within the ribosome, this orientation would place 3H1 near the peptidyltransferase center in an A-site-binding kl-TSS, a location that might not permit a 12-bp hairpin. This possibility led to the evaluation of a second orientation for the kl-TSS with respect to a canonical tRNA. Orientation B (Fig. 9C and D) places hairpin 3H1 in the anticodon stem position, which would position both the 12-bp interacting hairpin and the remainder of the viral RNA in the mRNA tunnel, where accommodation should be possible. In this orientation, hairpin 3H2 mimics the amino acid acceptor arm of a tRNA. Since both orientations appear to align the PEMV kl-TSS comparably well with a tRNA, imaging the ribosome-bound element via crystallography or cryo-EM will be necessary to discern between the two options.

The kl-TSS inhibits translation in *trans*. Previous studies reported that addition of the PTE in a 100-fold excess in *trans* inhibited translation of a heterologous reporter construct containing the *Barley yellow dwarf virus* (BTE) translation enhancer by 75% (30). The recent discovery that the PTE is adjacent to the kl-TSS suggested a need to revisit the prior study to determine if the high concentration of added PTE and the use of a heterologous reporter construct were necessary to achieve translational inhibition because of the absence of the kl-TSS. Using PEMV 5′89 and the 3′UTR to direct reporter gene translation, with a 10-fold molar excess of PTE and/or kl-TSS added in *trans*, the PTE had only a weak effect on translation (14%), whereas the kl-TSS reduced translation by 57%. Inclusion of a transcript containing the PTE and the kl-TSS resulted in a 75% reduction in translation (Fig. 2C). Since levels of inhibition can be proportional to the efficiency of translational enhancement when located in *cis* (30, 58–60), this

suggests that the kl-TSS may be the more dominant 3′CITE, with the role of the PTE being to assist in the recruitment of 80S ribosomes or ribosomal subunits to the kl-TSS in an eIF4E-dependent manner. Both RNA-RNA interaction and ribosome-binding activities of the kl-TSS contributed to translational inhibition when the kl-TSS was supplied in *trans* (Fig. 2), supporting our previous results indicating that both activities are important for kl-TSS 3′CITE function (12).

The kl-TSS and PTE were ineffective at enhancing translation when supplied in *trans* to a template with a kl-TSS disabled in either the RNA-RNA interaction or ribosome-binding activity, suggesting that these 3′CITEs must be in *cis* to function as translational enhancers. This is in contrast to the 3′CITE of *Maize necrotic streak virus*, which enhanced translation both in *cis* and in *trans* in WGE by rescuing the translation of a defective *Carnation Italian ringspot virus* template that lacked the 3′CITE (14). The inability of the kl-TSS to enhance translation in *trans* suggests that ribosome recruitment and transfer to the 5′ end are linked to *cis*-translation. Alternatively, additional 3′ elements may be required for full function of the kl-TSS/PTE translational enhancers.

In conclusion, the PEMV kl-TSS is a multifunctional 3′CITE that binds to ribosomes in a non-P-site location. Simultaneous binding of the kl-TSS to ribosomes and a 5′ proximal hairpin suggests a model whereby ribosomes or ribosomal subunits, either during the pioneer round of protein synthesis or once completing translation, bind to the kl-TSS in *cis* with support from the eIF4E-bound PTE. The bound ribosome may assist formation of the long-distance kissing-loop interaction, which circularizes the genome, delivering the kl-TSS-bound ribosomes to the 5′ end, which supports cap-independent translation initiation. The substantive differences between the PEMV kl-TSS and the TCV TSS suggest that tRNA mimics have evolved to utilize different mechanisms for translational enhancement.

ACKNOWLEDGMENTS

This work was supported by grants from the U.S. Public Health Service (GM 061515-05A2/G120CD and GM 061515-07S1) and the NSF (MCB 1157906) to A.E.S. and from the U.S. Public Health Service (GM 058859) to J.D.D. This publication was also funded in part by federal funds from the Frederick National Laboratory for Cancer Research, National Institutes of Health, under contract HHSN 261200800001E to W.K. This research was additionally supported in part by a grant from the Intramural Research Program of the National Institutes of Health, Center for Cancer Research, to B.A.S.

The content of this publication does not necessarily reflect the views or policies of the Department of Health and Human Services, nor does mention of trade names, commercial products, or organizations imply endorsement by the U.S. Government.

REFERENCES

1. **Sonenberg N, Hinnebusch AG.** 2009. Regulation of translation initiation in eukaryotes: mechanisms and biological targets. Cell **136:**731–745.
2. **Jackson RJ, Hellen CU, Pestova TV.** 2010. The mechanism of eukaryotic translation initiation and principles of its regulation. Nat. Rev. Mol. Cell. Biol. **11:**113–127.
3. **Sonenberg N.** 2008. eIF4E, the mRNA cap-binding protein: from basic discovery to translational research. Biochem. Cell Biol. **86:**178–183.
4. **Jacobson A.** 1996. Poly(A) metabolism and translation: the closed-loop model. Cold Spring Harbor Monogr. Ser. Transl. Control **30:**451–480.
5. **Wells SE, Hillner PE, Vale RD, Sachs AB.** 1998. Circularization of mRNA by eukaryotic translation initiation factors. Mol. Cell **2:**135–140.
6. **Spriggs KA, Bushell M, Willis AE.** 2010. Translational regulation of gene expression during conditions of cell stress. Mol. Cell **40:**228–237.
7. **Mokrejs M, Masek T, Vopalensky V, Hlubucek P, Delbos P, Pospisek M.** 2010. IRESite—a tool for the examination of viral and cellular internal ribosome entry sites. Nucleic Acids Res. **38:**D131–D136.
8. **Kieft JS.** 2008. Viral IRES RNA structures and ribosome interactions. Trends Biochem. Sci. **33:**274–283.
9. **Nicholson BL, White KA.** 2011. 3′ cap-independent translation enhancers of positive-strand RNA plant viruses. Curr. Opin. Virol. **1:**373–380.
10. **Kneller EL, Rakotondrafara AM, Miller WA.** 2006. Cap-independent translation of plant viral RNAs. Virus Res. **119:**63–75.
11. **Simon AE, Miller WA.** 2013. 3′ cap-independent translation enhancers of plant viruses. Annu. Rev. Microbiol. **67:**21–42.
12. **Gao F, Kasprzak W, Stupina VA, Shapiro BA, Simon AE.** 2012. A ribosome-binding, 3′ translational enhancer has a T-shaped structure and engages in a long-distance RNA-RNA interaction. J. Virol. **86:**9828–9842.
13. **Chattopadhyay M, Shi K, Yuan X, Simon AE.** 2011. Long-distance kissing loop interactions between a 3′ proximal Y-shaped structure and apical loops of 5′ hairpins enhance translation of Saguaro cactus virus. Virology **417:**113–125.
14. **Nicholson BL, Wu B, Chevtchenko I, White KA.** 2010. Tombusvirus recruitment of host translational machinery via the 3′ UTR. RNA **16:**1402–1419.
15. **Miller WA, White KA.** 2006. Long-distance RNA-RNA interactions in plant virus gene expression and replication. Annu. Rev. Phytopathol. **44:**447–467.
16. **Kozak M.** 1989. The scanning model for translation: an update. J. Cell Biol. **108:**229–241.
17. **Cigan AM, Feng L, Donahue TF.** 1988. tRNAi(met) functions in directing the scanning ribosome to the start site of translation. Science **242:**93–97.
18. **Kozak M.** 1978. How do eucaryotic ribosomes select initiation regions in messenger RNA? Cell **15:**1109–1123.
19. **Dreher TW.** 2009. Role of tRNA-like structures in controlling plant virus replication. Virus Res. **139:**217–229.
20. **Jones CP, Saadatmand J, Kleiman L, Musier-Forsyth K.** 2013. Molecular mimicry of human tRNALys anti-codon domain by HIV-1 RNA genome facilitates tRNA primer annealing. RNA **19:**219–229.
21. **Baumstark T, Ahlquist P.** 2001. The brome mosaic virus RNA3 intergenic replication enhancer folds to mimic a tRNA TpsiC-stem loop and is modified in vivo. RNA **7:**1652–1670.
22. **Costantino DA, Pfingsten JS, Rambo RP, Kieft JS.** 2008. tRNA-mRNA mimicry drives translation initiation from a viral IRES. Nat. Struct. Mol. Biol. **15:**57–64.
23. **Stupina VA, Meskauskas A, McCormack JC, Yingling YG, Shapiro BA, Dinman JD, Simon AE.** 2008. The 3′ proximal translational enhancer of Turnip crinkle virus binds to 60S ribosomal subunits. RNA **14:**2379–2393.
24. **Zuo XB, Wang JB, Yu P, Eyler D, Xu H, Starich MR, Tiede DM, Simon AE, Kasprzak W, Schwieters CD, Shapiro BA, Wang YX.** 2010. Solution structure of the cap-independent translational enhancer and ribosome-binding element in the 3′ UTR of turnip crinkle virus. Proc. Natl. Acad. Sci. U. S. A. **107:**1385–1390.
25. **McCormack JC, Yuan X, Yingling YG, Kasprzak W, Zamora RE, Shapiro BA, Simon AE.** 2008. Structural domains within the 3′ untranslated region of Turnip crinkle virus. J. Virol. **82:**8706–8720.
26. **de Zoeten GA, Skaf JS.** 2001. Pea enation mosaic and the vagaries of a plant virus. Adv. Virus Res. **57:**323–350.
27. **Demler SA, Rucker DG, de Zoeten GA.** 1993. The chimeric nature of the genome of pea enation mosaic virus: the independent replication of RNA 2. J. Gen. Virol. **74:**1–14.
28. **Batten JS, Desvoyes B, Yamamura Y, Scholthof KB.** 2006. A translational enhancer element on the 3′-proximal end of the Panicum mosaic virus genome. FEBS Lett. **580:**2591–2597.
29. **Wang Z, Treder K, Miller WA.** 2009. Structure of a viral cap-independent translation element that functions via high affinity binding to the eIF4E subunit of eIF4F. J. Biol. Chem. **284:**14189–14202.
30. **Wang Z, Parisien M, Scheets K, Miller WA.** 2011. The cap-binding translation initiation factor, eIF4E, binds a pseudoknot in a viral cap-independent translation element. Structure **19:**868–880.
31. Reference deleted.
32. **Stupina VA, Simon AE.** 2013. Preparation of biologically active Arabidopsis ribosomes and comparison with yeast ribosomes for binding to a tRNA-mimic that enhances translation of plant plus-strand RNA viruses. Front. Plant Sci. **4:**271. doi:10.3389/fpls.2013.

33. **Leshin JA, Heselpoth R, Belew AT, Dinman JD.** 2011. High throughput structural analysis of yeast ribosomes using hSHAPE. RNA Biol. **8:**478–487.
34. **Triana F, Nierhaus KH, Chakraburtty K.** 1994. Transfer RNA binding to 80S ribosomes from yeast: evidence for three sites. Biochem. Mol. Biol. Int. **33:**909–915.
35. **Yuan XF, Shi KR, Meskauskas A, Simon AE.** 2009. The 3′ end of Turnip crinkle virus contains a highly interactive structure including a translational enhancer that is disrupted by binding to the RNA-dependent RNA polymerase. RNA **15:**1849–1864.
36. **Martinez HM, Maizel JV, Jr, Shapiro BA.** 2008. RNA2D3D: a program for generating, viewing, and comparing 3-dimensional models of RNA. J. Biomol. Struct. Dyn. **25:**669–683.
37. **Parisien M, Major F.** 2008. The MC-Fold and MC-Sym pipeline infers RNA structure from sequence data. Nature **452:**51–55.
38. **Case DA, Darden TA, Cheatham TEI, Simmerling CL, Wang J, Duke RE, Luo R, Walker RC, Zhang W, Merz KM, Roberts B, Hayik S, Roitberg A, Seabra G, Swails J, Goetz AW, Kolossváry I, Wong KF, Paesani F, Vanicek J, Wolf RM, Liu J, Wu X, Brozell SR, Steinbrecher T, Gohlke H, Cai Q, Ye X, Wang J, Hsieh M-J, Cui G, Roe DR, Mathews DH, Seetin MG, Salomon-Ferrer R, Sagui C, Babin V, Luchko T, Gusarov S, Kovalenko A, Kollman PA.** 2012. Amber 12. University of California, San Francisco, CA.
39. **Essmann U, Perera L, Berkowitz ML, Darden T, Lee H, Pedersen LG.** 1995. A smooth particle mesh EWALD method. J. Chem. Phys. **103:**8577–8593.
40. **Wang J, Cieplak P, Kollman PA.** 2000. How well does a restrained electrostatic potential (RESP) model perform in calculating conformational energies of organic and biological molecules? J. Comput. Chem. **21:**1049–1074.
41. **Berendsen HJC, Postma JPM, van Gunsteren WF, DiNola A, Haak JR.** 1984. Molecular dynamics with coupling to an external bath. J. Chem. Phys. **1984:**3684–3690.
42. **Nicholson BL, White KA.** 2008. Context-influenced cap-independent translation of Tombusvirus mRNAs in vitro. Virology **380:**203–212.
43. **Soukup GA, Breaker RR.** 1999. Relationship between internucleotide linkage geometry and the stability of RNA. RNA **5:**1308–1325.
44. **Wilkinson KA, Merino EJ, Weeks KM.** 2006. Selective 2′-hydroxyl acylation analyzed by primer extension (SHAPE): quantitative RNA structure analysis at single nucleotide resolution. Nat. Protoc. **1:**1610–1616.
45. **Vasa SM, Guex N, Wilkinson KA, Weeks KM, Giddings MC.** 2008. ShapeFinder: a software system for high-throughput quantitative analysis of nucleic acid reactivity information resolved by capillary electrophoresis. RNA **14:**1979–1990.
46. **Wilkinson KA, Gorelick RJ, Vasa SM, Guex N, Rein A, Mathews DH, Giddings MC, Weeks KM.** 2008. High-throughput SHAPE analysis reveals structures in HIV-1 genomic RNA strongly conserved across distinct biological states. PLoS Biol. **6:**883–899.
47. **Demeshkina N, Jenner L, Yusupova G, Yusupov M.** 2010. Interactions of the ribosome with mRNA and tRNA. Curr. Opin. Struct. Biol. **20:**325–332.
48. **Valle M, Zavialov A, Li W, Stagg SM, Sengupta J, Nielsen RC, Nissen P, Harvey SC, Ehrenberg M, Frank J.** 2003. Incorporation of aminoacyl-tRNA into the ribosome as seen by cryo-electron microscopy. Nat. Struct. Biol. **10:**9–906.
49. **Schluenzen F, Tocilj A, Zarivach R, Harms J, Gluehmann M, Janell D, Bashan A, Bartels H, Agmon I, Franceschi F, Yonath A.** 2000. Structure of functionally activated small ribosomal subunit at 3.3 angstrom resolution. Cell **102:**615–623.
50. **Meskauskas A, Dinman JD.** 2007. Ribosomal protein L3: gatekeeper to the A site. Mol. Cell **25:**877–888.
51. **Miller WA, Wang Z, Treder K.** 2007. The amazing diversity of cap-independent translation elements in the 3′-untranslated regions of plant viral RNAs. Biochem. Soc. Trans. **35:**1629–1633.
52. **Stupina VA, Yuan X, Meskauskas A, Dinman JD, Simon AE.** 2011. Ribosome binding to a 5′ translational enhancer is altered in the presence of the 3′ untranslated region in cap-independent translation of turnip crinkle virus. J. Virol. **85:**4638–4653.
53. **Rakotondrafara AM, Polacek C, Harris E, Miller WA.** 2006. Oscillating kissing stem-loop interactions mediate 5′ scanning-dependent translation by a viral 3′-cap-independent translation element. RNA **12:**1893–1906.
54. **Kraft JJ, Treder K, Peterson MS, Miller WA.** 2013. Cation-dependent folding of 3′ cap-independent translation elements facilitates interaction of a 17-nucleotide conserved sequence with eIF4G. Nucleic Acids Res. **41:**3398–3413.
55. **Demeshkina N, Jenner L, Westhof E, Yusupov M, Yusupova G.** 2012. A new understanding of the decoding principle on the ribosome. Nature **484:**256–259.
56. **Ortiz-Meoz RF, Green R.** 2011. Helix 69 is key for uniformity during substrate selection on the ribosome. J. Biol. Chem. **286:**25604–25610.
57. **O'Connor M.** 2009. Helix 69 in 23S rRNA modulates decoding by wild type and suppressor tRNAs. Mol. Gen. Genet. **282:**371–380.
58. **Wang Z, Kraft JJ, Hui AY, Miller WA.** 2010. Structural plasticity of Barley yellow dwarf virus-like cap-independent translation elements in four genera of plant viral RNAs. Virology **402:**177–186.
59. **Gazo BM, Murphy P, Gatchel JR, Browning KS.** 2004. A novel interaction of cap-binding protein complexes eukaryotic initiation factor (eIF)4F and eIF(iso)4F with a region in the 3′-untranslated region of satellite tobacco necrosis virus. J. Biol. Chem. **279:**13584–13592.
60. **Guo L, Allen E, Miller WA.** 2000. Structure and function of a cap-independent translation element that functions in either the 3′ or the 5′ untranslated region. RNA **6:**1808–1820.